Reconfigurable Antennas Enabled by Tunable Metasurfaces for Next-Generation Wireless Communications: A Review

electronics

MDPI

Review

Reconfigurable Antennas Enabled by Tunable Metasurfaces for Next-Generation Wireless Communications: A Review

Zahra Hamzavi-Zarghani [1,*], Ladislau Matekovits [2,3,4] and Wolfgang Bösch [1]

[1] Institute of Microwave and Photonic Engineering, Graz University of Technology, 8010 Graz, Austria; wbosch@tugraz.at
[2] Department of Electronics and Telecommunications, Politecnico di Torino, 10129 Turin, Italy; ladislau.matekovits@polito.it
[3] Department of Measurements and Optical Electronics, Politehnica University Timisoara, 300006 Timişoara, Romania
[4] Istituto di Elettronica e di Ingegneria dell'Informazione e delle Telecomunicazioni, National Research Council, 10129 Turin, Italy
* Correspondence: zahra.hamzavizarghani@tugraz.at

Abstract

Reconfigurable antennas play a central role in next-generation wireless communication systems by enabling dynamic adaptation of operating frequency, radiation pattern, and polarization. Tunable metasurfaces have emerged as a powerful and compact approach to antenna reconfiguration, allowing electromagnetic wave manipulation through engineered, planar structures whose properties can be dynamically controlled. By embedding active devices or tunable materials within metasurface unit cells, antenna characteristics can be modified without altering the antenna geometry. This review provides a comprehensive overview of reconfigurable antennas enabled by tunable metasurfaces. We adopt a functionality-based classification that focuses on operating frequency, radiation pattern, polarization, and multifunction reconfiguration. An overview of major tunability technologies, including PIN diodes, varactors, MEMS, graphene and two-dimensional materials, and liquid crystal (LC) or phase-change materials, is first presented. Subsequently, metasurface-based reconfiguration strategies are discussed and compared for each antenna functionality, highlighting design principles, practical trade-offs, and limitations. The review concludes with an assessment of challenges and future research directions relevant to next-generation wireless communications and beyond.

Keywords: antenna; tunability; reconfigurability; metasurface

Academic Editor: Ikmo Park

Received: 2 March 2026
Revised: 1 April 2026
Accepted: 3 April 2026
Published: 13 April 2026

1. Introduction

The rapid development of wireless systems in terms of data rate, spectrum flexibility, and network diversity has driven a rising demand for antennas capable of adaptive operation. Traditional fixed antennas, optimized for a single band, pattern, or polarization, are not suitable for systems in which channel conditions, spectrum availability, or operating requirements change. Reconfigurable antennas address these challenges by enabling dynamic modification of key electromagnetic characteristics, thereby improving spectral efficiency, reducing hardware redundancy, and enhancing system flexibility [1,2]. Such capabilities make reconfigurable antennas well-suited to advanced wireless systems. By providing multiple operational modes within one structure, they can replace several dedicated antennas, yielding notable reductions in size and expense, while simplifying system-level integration and improving overall performance [3,4].

Early reconfigurable antenna designs typically involved altering the radiating element or feed network with switches such as PIN diodes, RF-MEMS, or mechanically actuated structures to change resonant frequency, pattern, or polarization [5–8]. These techniques can significantly perturb the current distribution, increase mechanical and electrical complexity, and limit scalability when multiple degrees of reconfiguration are required [6]. The limitations of direct radiator modification prompted a conceptual shift in antenna reconfiguration strategy. Instead of embedding tunable elements into the antenna itself, researchers began to investigate approaches that modify the electromagnetic boundary conditions surrounding the antenna. This led to the development of metasurfaces to enable precise control over reflected, transmitted, or radiated waves. By offering reconfiguration without altering the radiator itself, metasurfaces provide a flexible platform for multifunctional and adaptive antenna systems [9–14].

The foundations of metasurfaces originate from decades of research into engineered planar structures capable of manipulating electromagnetic fields. Initial research on frequency-selective surfaces demonstrated that periodic, subwavelength apertures or patches patterned on a surface could selectively transmit or reflect incident waves, revealing the potential for controllable boundary-layer electromagnetics [15–17]. In the late 1990s, the development of high-impedance surfaces and electromagnetic bandgap (EBG) structures, most notably Sievenpiper's "mushroom" configuration, introduced planar artificial magnetic conductors (AMCs) that supported surface-wave suppression and in-phase reflection [18–20]. These studies established the possibility that engineered surfaces, rather than bulky volumetric structures, could serve as functional electromagnetic interfaces [21–23].

A major shift emerged when researchers realized that patterned surfaces could be systematically engineered to control electromagnetic wavefronts. It was shown that arrays of subwavelength elements are capable of introducing engineered phase, amplitude, or polarization changes, establishing generalized laws of reflection and refraction [24–26]. This finding demonstrated that a single thin layer could realize functions previously feasible only with bulk metamaterials, driving the rapid expansion of metasurface research across the electromagnetic spectrum [27].

Progress during the following decade shaped metasurfaces into a coherent scientific framework. Holloway and co-workers formalized electromagnetic models capable of treating metasurfaces as generalized impedance or susceptibility boundaries, providing a unified theoretical language applicable across frequency bands, device types, and implementations [28]. Glybovski et al. then compiled the various conceptual, analytical, and technological threads into a widely referenced review that established common definitions, classifications, and performance metrics, helping metasurfaces emerge as a distinct research discipline [29].

Parallel advances broadened the functional scope of metasurfaces beyond conventional reflection-phase engineering. Alù and Engheta first established tunable scattering control using nanocircuit-loaded optical inclusions, introducing the meta-atom concepts that later enabled ultrathin cloaking implementations [30]. These ideas were realized in practice through the mantle cloaking metasurface concept, where patterned two-dimensional coatings suppress scattering without volume metamaterials [31–35]. Complementary work on Huygens metasurfaces further showed that properly designed metasurfaces can balance electric and magnetic responses to support reflectionless transmission and highly efficient wavefront transformation [36,37]. Collectively, these developments reshaped metasurfaces from patterned conducting sheets into versatile platforms capable of sophisticated wave manipulation, including cloaking, beam control, and multifunctional field transformations [38–40].

With metasurface capabilities firmly established, metasurfaces rapidly migrated from conceptual demonstrations to antenna technology, where their ability to engineer boundary conditions and suppress unwanted radiation proved significant [9,41]. Patterned surfaces that tailor local phase, amplitude, and polarization responses can improve key antenna characteristics, such as gain enhancement [42,43], bandwidth improvement [44,45] impedance matching [46,47], suppression of surface-wave losses [48,49], radar cross-section (RCS) reduction [50,51], and reduction in back radiation and miniaturization [52,53], while also enabling directive beam formation without the need for bulky structures [54–58]. More recently, the incorporation of active materials, tunable meta-atoms, and embedded biasing networks has enabled reconfigurable metasurface antennas capable of dynamically modifying beam direction, operating frequency, or polarization without altering the physical footprint of the radiating element [14,59–64]. These advances position metasurfaces not only as passive enhancing layers but also as fully reconfigurable interfaces that can adapt antenna behavior in real time for emerging wireless, sensing, and communication applications [13,65–67].

This paper reviews reconfigurable antennas enabled by tunable metasurfaces and summarizes recent advances across four major capability areas: frequency tuning, radiation pattern control, polarization switching, and multifunctional operation. Representative designs and implementation strategies are discussed, along with associated performance considerations, trade-offs, and practical limitations. The review concludes with emerging directions and opportunities that position tunable metasurface-based antennas as promising candidates for future wireless communication systems.

2. Fundamentals of Metasurface-Enabled Antenna Reconfiguration

Metasurfaces are two-dimensional arrangements of subwavelength scattering elements engineered to enforce customized electromagnetic boundary conditions. Each unit cell interacts locally with the incident field and produces a controllable phase, amplitude, or polarization response. When assembled into periodic or quasi-periodic structures, the collective behavior of these unit cells enables precise manipulation of reflected, transmitted, or guided electromagnetic waves [68–72].

2.1. Wavefront Manipulation Using Engineered Phase Gradients

A key capability of metasurfaces lies in their ability to enforce intentionally engineered phase gradients along the plane of interaction. Rather than obeying classical Snell's law, metasurfaces can redirect reflected and transmitted beams according to generalized refraction and reflection laws due to the engineered phase gradient along the surface [24,73].

Figure 1 illustrates this concept for a planar metasurface illuminated by an incident plane wave. The metasurface lies in the x-y plane and enforces a controllable phase distribution $\Phi(x, y)$. When the surface imparts a nonuniform phase response, characterized by gradients $\partial\Phi/\partial x$ and $\partial\Phi/\partial y$, the reflected and transmitted beams are deflected into anomalous directions, distinct from the ordinary angles predicted by conventional refractive behavior. The generalized laws of refraction for such anisotropic boundary conditions are given by [73]:

$$\begin{cases} n_t \sin(\theta_t) - n_i \sin(\theta_i) = \dfrac{1}{k_0} \dfrac{\partial \Phi}{\partial x} \\ \cos(\theta_t) \sin(\varphi_t) = \dfrac{1}{n_t k_0} \dfrac{\partial \Phi}{\partial y} \end{cases} \tag{1}$$

$$\begin{cases} \sin(\theta_r) - \sin(\theta_i) = \dfrac{1}{n_i k_0} \dfrac{\partial \Phi}{\partial x} \\ \cos(\theta_r) \sin(\varphi_r) = \dfrac{1}{n_r k_0} \dfrac{\partial \Phi}{\partial y} \end{cases} \tag{2}$$

where n_i, n_t, and n_r are the refractive indices of the incident, transmitted, and reflected media, respectively, and k_0 is the free-space wavenumber.

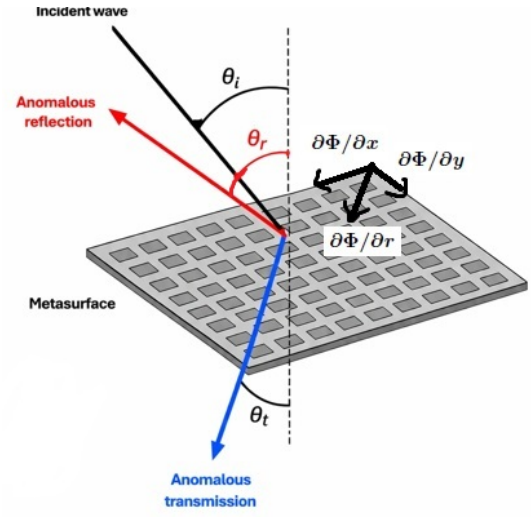

Figure 1. Schematic illustration of generalized reflection and refraction at a planar metasurface, adapted from: [73].

As illustrated, a nonzero phase gradient forces the reflected beam to deviate into an anomalous reflection direction (red arrow) and drives the transmitted field toward an anomalous refraction path (blue arrow). This generalized behavior enables metasurfaces to perform beam steering, focusing, multi-beam generation, and other transformations using a single ultrathin layer.

2.2. Roles of Metasurfaces in Antenna Structures

In antenna systems, metasurfaces may be incorporated in several geometries depending on the desired functionality:

(1) Superstrate loading
Placed above a radiator to modify aperture illumination, enhance gain, or control the far-field pattern [74,75].

(2) Reflectarray or transmitarray configurations
Arrays of phase-gradient elements act as compact reflectors or lenses, replacing bulky antennas while enabling beam steering or multi-beam generation [76,77].

(3) Engineered ground planes (AMCs/EBGs)
High-impedance or bandgap structures suppress surface waves, reduce back radiation, and lower physical profile [78,79].

(4) Near-field parasitic coupling layers
Patterned surfaces located within the near-field region modify resonance, impedance, and polarization without altering the radiator geometry [80,81].

In all configurations, antenna performance results from electromagnetic coupling between the radiator and the engineered boundary conditions imposed by the metasurface.

2.3. Tunable Metasurfaces for Antenna Reconfiguration

Static metasurfaces exhibit fixed electromagnetic responses. Introducing tunability allows the surface boundary conditions to be dynamically modified, enabling real-time control of antenna characteristics. In practice, this is achieved by embedding controllable elements or materials within the metasurface unit cells, allowing adjustment of effective surface impedance, phase response, or anisotropy. Such tunable metasurfaces form the foundation for reconfigurable antenna operation, enabling dynamic control of frequency,

radiation pattern, and polarization [9,60,82–87]. Detailed implementations and tuning mechanisms are discussed in later sections.

3. Overview of Tunable Metasurface Technologies

This section provides an overview of the major technologies used to realize tunable metasurfaces in antenna applications. The discussion focuses on physical operating principles, advantages, and practical limitations.

3.1. Semiconductor-Based Tuning: PIN Diodes and Varactors

PIN diodes are widely employed as RF switches due to their ability to switch between low-resistance (ON) and high-impedance (OFF) states under forward and reverse bias conditions [88–90]. When integrated into metasurface unit cells, they enable discrete reconfiguration by modifying current distribution and surface impedance. This makes them particularly suitable for applications such as beam switching, polarization reconfiguration, and multi-state operation requiring fast and reliable transitions. However, their discrete nature limits tuning resolution, and the presence of parasitic resistance and inductance can introduce losses, especially at higher frequencies [91,92].

Varactor diodes provide continuous tuning through voltage-dependent junction capacitance. By adjusting the reverse bias voltage, the effective capacitance varies, enabling smooth control of resonant frequency and phase response [89,93]. This property makes varactors attractive for applications such as continuous beam steering and frequency tuning. However, they generally introduce higher losses compared to PIN diodes and require more complex biasing networks, particularly in densely packed metasurface arrays. A direct quantitative comparison between PIN-diode- and varactor-based metasurfaces is difficult, as the reported loss strongly depends on the specific unit-cell design, operating frequency, and implementation details. Nevertheless, it is generally observed that PIN-diode-based approaches exhibit lower loss, whereas varactor-based designs tend to introduce higher loss, particularly at millimeter-wave frequencies [94–98].

3.2. RF-MEMS-Based Tunable Metasurfaces

RF-MEMS devices achieve reconfiguration through mechanically controlled variations in circuit geometry, typically using movable membranes actuated by electrostatic forces. Because they do not rely on semiconductor carrier transport, RF-MEMS devices exhibit very low insertion loss, high linearity, and excellent RF performance across microwave and millimeter-wave frequencies [99–104].

These characteristics make RF-MEMS particularly attractive for high-efficiency metasurface antennas. However, their switching speed is limited by mechanical motion, typically in the microsecond range ($\approx$1–100 µs), which is significantly slower than semiconductor-based tuning mechanisms. This limited response speed can restrict their performance in applications that require rapid beam reconfiguration, such as real-time beam tracking in dynamic wireless environments and adaptive MIMO systems. In addition, their fabrication and packaging processes are more complex than those of semiconductor-based solutions, while reliability and cost considerations remain important challenges for large-scale implementations [105–110].

3.3. Liquid-Crystal-Based Tunable Metasurfaces

Liquid crystals enable continuous tunability by exploiting electrically controlled molecular reorientation, which modifies the effective permittivity of the medium. This allows smooth adjustment of the metasurface response without altering the physical structure. Such behavior is particularly advantageous for applications that require analog phase control, such as beam steering and reconfigurable reflectarrays [111–118].

Liquid-crystal-based metasurfaces typically exhibit low power consumption and relatively simple biasing schemes. However, their tuning speed is limited by molecular dynamics and is generally in the millisecond range, thereby restricting their applicability to fast, real-time reconfigurable systems [117,119–121]. This limitation originates from the physical reorientation of liquid crystal molecules, which directly governs the update speed of the effective permittivity and, consequently, the electromagnetic response of the metasurface. Because this process occurs on a millisecond timescale, the metasurface cannot track rapid changes in beam direction or polarization, restricting its use in fast-switching applications.

Despite the progress in liquid-crystal-based tunable metasurfaces, several research gaps remain. One major limitation is the relatively slow response time associated with molecular reorientation, which restricts their use in fast and real-time reconfigurable systems. In addition, achieving uniform and stable alignment of liquid crystal molecules over large apertures remains challenging, particularly in complex biasing configurations. Another open challenge is the integration of LC layers with compact and low-loss metasurface designs, especially at higher frequencies, where material losses and fabrication tolerances become more critical. Furthermore, improving the long-term stability and environmental robustness of LC-based devices is still an important research direction for practical deployment.

3.4. Phase-Change-Material-Based Tunable Metasurfaces

Phase-change materials (PCMs), such as vanadium dioxide (VO_2) and chalcogenide alloys such as $Ge_2Sb_2Te_5$ (GST), enable reconfiguration through reversible transitions between distinct material states with significantly different electrical properties. These transitions result in substantial changes in conductivity and permittivity, allowing strong modulation of resonance and wave interaction [122–130].

PCM-based metasurfaces are particularly effective for applications such as frequency switching, dual-mode operation, and multifunctional devices. Their ability to maintain a given state without continuous biasing (nonvolatile behavior) is a key advantage [83,126,131–139]. However, they also have significant limitations. The switching process may lead to performance degradation and reliability issues under repeated switching operations. In addition, thermal or electrical activation increases power consumption and complicates system integration. Their relatively slow switching speed compared to electronic approaches also limits their use in real-time applications. Therefore, although PCMs are promising, their use in large-scale and high-speed systems is still under development [129,140–142]. In addition, achieving a uniform phase transition across large metasurface apertures is challenging due to thermal nonuniformity, where spatial temperature variations can lead to incomplete or uneven switching of the material. To mitigate this issue, several thermal management strategies have been explored, including the use of uniform heating schemes, thermally conductive substrates or layers to improve heat spreading, and localized heating elements for more precise control of the phase transition. Multilayer structures and optimized thermal design can further help reduce temperature gradients across the aperture. Despite these efforts, their relatively slow switching speed compared to electronic approaches still limits their use in real-time applications. Therefore, although PCMs are promising, their use in large-scale and high-speed systems is still under development [143,144].

3.5. Graphene and Other Two-Dimensional Materials

Graphene and related two-dimensional materials offer electrically controlled tunability through modulation of carrier density. By adjusting the Fermi level via electrostatic gating, their surface conductivity can be continuously tuned, enabling dynamic control of amplitude, phase, and polarization response [145–152].

These materials are particularly promising for terahertz and higher-frequency applications, where strong light–matter interaction enables compact and efficient tunable metasurfaces. They provide continuous and reversible tuning with potentially very fast intrinsic response [153–157]. Despite these advantages, graphene-based metasurfaces still face several practical challenges. Their performance strongly depends on material quality and fabrication processes, which remain difficult to control over large areas. In addition, biasing and integration of graphene in large arrays can be complex, and losses can be significant depending on the operating frequency. As a result, most graphene-based implementations are still at the laboratory stage and require further development for large-scale practical deployment [158,159].

For graphene-based metasurfaces, the static bias power is generally very low because the tuning is mainly capacitive. Ideally, each unit cell consumes nearly zero static power, and the main contribution comes from small leakage currents in the bias network. For large, continuously tuned apertures, the total static power increases with the number of unit cells due to this accumulated leakage. Therefore, while the power per unit cell is very small, the overall power consumption can become noticeable in large arrays. As a result, the main challenge is not the intrinsic power of graphene but the scalability of the biasing network and leakage control [160–162].

In addition to the discussed approaches, chemical reconfiguration has also been explored as an alternative tuning mechanism. In this approach, the electromagnetic properties of the metasurface are modified through chemical processes such as doping, adsorption of molecules, or electrochemical reactions, which alter the material's conductivity or permittivity. While this method can enable large and sometimes nonvolatile changes in material response, it typically suffers from slow response times, limited reversibility, and challenges in precise control. As a result, chemical reconfiguration remains less developed for real-time tunable metasurface antenna applications [163].

At terahertz frequencies, graphene-based and other two-dimensional material platforms are among the most promising candidates for implementing reconfigurable metasurfaces due to their strong light–matter interaction and electrically tunable conductivity. However, their performance is still limited by material losses and fabrication challenges. Alternatively, liquid crystals and phase-change materials can provide larger modulation depth, but their relatively slow response time restricts their use in dynamic applications. Therefore, the most suitable approach depends on the specific application requirements, with graphene-based solutions being particularly attractive for fast and continuously tunable THz metasurfaces [129].

Table 1 summarizes and compares the main tunable metasurface technologies in terms of key performance parameters, including tuning type, switching speed, insertion loss, tuning resolution, biasing complexity, and integration considerations. This comparison highlights the inherent trade-offs among different approaches and facilitates the selection of appropriate tuning mechanisms for specific antenna applications.

Table 1. Comparative summary of the main tunable metasurface technologies used in antenna applications. The reported values represent typical ranges observed in the literature and may vary depending on device design, material properties, and operating conditions.

Technology	Freq.	Loss	Speed	Resolution	Biasing	Applications
PIN diodes	MHz–mmWave	Mod.–high	1–100 ns	Binary	1–5 V	Beam/polarization switching
Varactors	MHz–mmWave	Mod.–high	1 ns–1 µs	High	1–20 V	Beam steering, freq. tuning
RF-MEMS	GHz–mmWave	Low	1–100 µs	Med.–high	20–80 V	Low-loss arrays
LCs	GHz–THz	Low–mod.	1–10 ms	High	1–10 V	Reflectarrays, phase shifters
PCMs	GHz–THz	Moderate	10 µs–1 ms	Medium	1–10 V	Frequency switching, reconfigurable antennas
Graphene	THz–optical	Moderate	1–100 ps	High	1–5 V	THz beam steering, tunable absorbers

3.6. General Tunable Metasurface Design Methodology

To provide a clear overview of the design process of tunable metasurfaces, Figure 2 presents the general workflow from electromagnetic specifications to fabrication. The design begins with specifying the electromagnetic performance, followed by the estimation of physical parameters, incorporating appropriate tuning mechanisms and materials, and the design of unit cells and array configurations. The process is then refined through iterative simulation and optimization, where feedback from both numerical simulations and experimental measurements is used to achieve the desired performance.

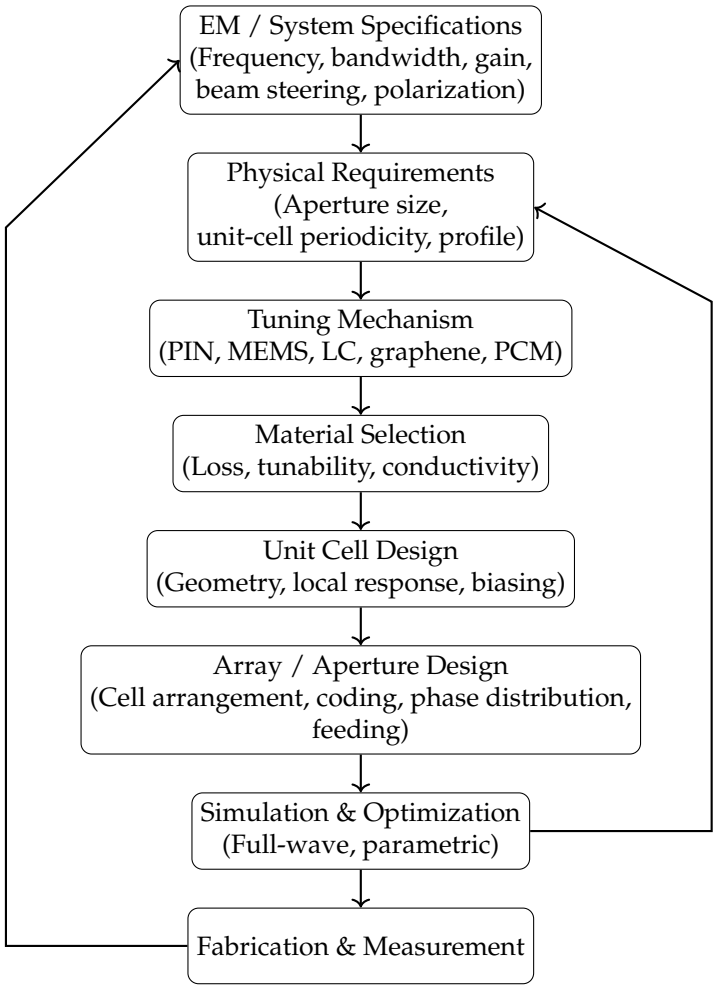

Figure 2. Design flow of tunable metasurfaces from specifications to fabrication.

The performance characteristics of different tuning mechanisms, such as switching speed, insertion loss, and tuning resolution, directly determine how effectively the electromagnetic response of each unit cell can be controlled. Since metasurface antenna functionalities arise from the collective response of these unit cells, the choice of tuning mechanism fundamentally governs the achievable reconfigurable behaviors, including beam steering, frequency tuning, and polarization control. Therefore, the following section discusses how these tuning technologies translate into specific functional reconfigurations in practical antenna systems.

4. Applications of Tunable Metasurfaces in Reconfigurable Antennas

Beyond their role as tunable electromagnetic surfaces, metasurfaces have enabled a wide range of reconfigurable antenna functionalities by engineering the electromagnetic environment surrounding the radiator. By appropriately designing and tuning the meta-

surface response, antenna characteristics such as operating frequency, radiation pattern, and polarization can be dynamically controlled without directly modifying the radiating element [164]. In recent years, increasing attention has been devoted to system-level implementations and real-time operation of tunable metasurface-based antennas [165–167]. This section reviews the major applications of tunable metasurfaces in reconfigurable antenna systems.

4.1. Radiation Pattern Reconfiguration and Beam Steering

Radiation pattern reconfiguration is one of the most prominent applications of tunable metasurfaces in antenna systems. By dynamically controlling the phase or amplitude distribution across the metasurface aperture, the main beam direction can be steered or reshaped without mechanical movement or complex phased-array feeding networks [100,168,169].

In [170], a two-dimensional steerable reflectarray based on LC technology is developed for reconfigurable intelligent surface (RIS) applications. The metasurface consists of an LC-loaded reflectarray aperture in which the phase response of each unit cell is controlled through applied bias voltages. The beam-steering principle is conceptually depicted in Figure 3a, where different voltage states applied to the LC elements generate a two-dimensional phase gradient, leading to dynamic beam deflection in both azimuth and elevation planes.

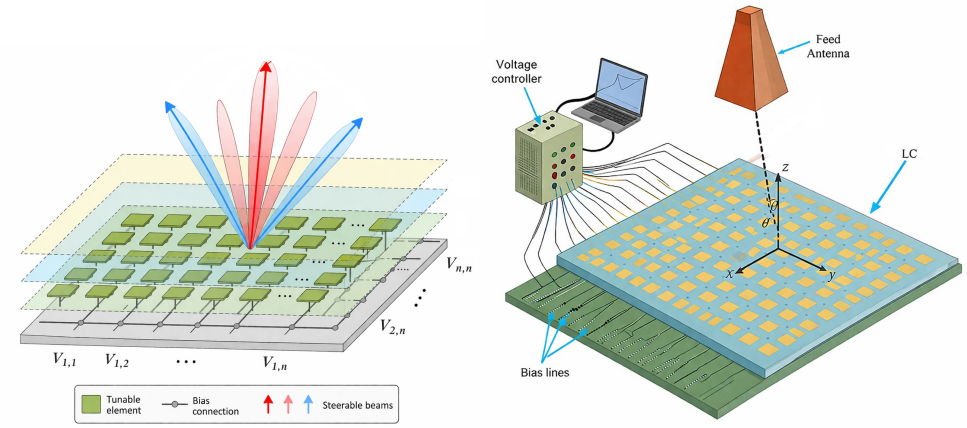

(**a**) (**b**)

Figure 3. Liquid-crystal-based two-dimensional steerable reflectarray. (**a**) Schematic of the LC unit-cell array with individually addressable bias voltages. (**b**) System-level configuration of the LC reflectarray, both adapted from [170].

Recently, metasurface-based RF signal modulation and programmable beamforming have attracted increasing attention for secure communication applications, enabling new strategies for physical-layer security and adaptive transmission control [171,172].

In Figure 3b, the overall configuration of the LC-based reflectarray is illustrated, including the feed antenna, voltage controller, and distributed biasing network. A horn antenna illuminates the reflectarray aperture, while the voltage controller applies individually controlled bias voltages to the LC unit cells through patterned bias lines. The LC layer is integrated within each reflectarray element, and its effective permittivity is tuned by the applied electric field across the cell. This configuration enables spatially varying phase control across the aperture, allowing the reflected beam to be electronically steered in two dimensions.

In [173], a tunable metasurface reflectarray antenna is reported for radiation pattern reconfiguration and beam steering. The use of varactor-based tuning elements within the

metasurface unit cells enables electrical control of the antenna radiation characteristics, allowing the main beam direction to be adjusted electrically.

The unit-cell configuration and metasurface layout are shown in Figure 4a, while the corresponding radiation patterns for different tuning states are presented in Figure 4b. The experimental results demonstrate continuous beam steering with stable gain, confirming the effectiveness of varactor-tuned metasurfaces in reconfigurable beam steering antennas.

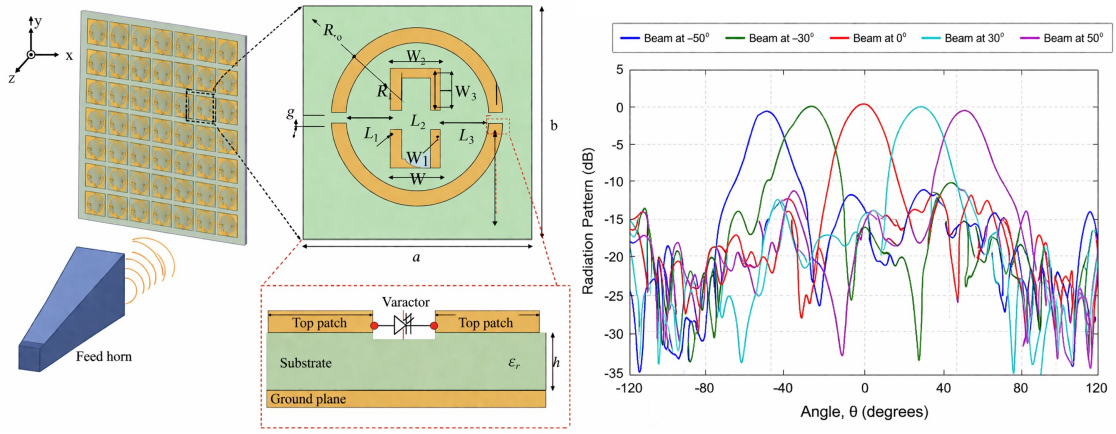

(**a**) (**b**)

Figure 4. Varactor-tuned metasurface reflectarray antenna for beam steering: (**a**) metasurface reflectarray configuration and unit-cell geometry, adapted from [173]; (**b**) Representative radiation patterns adapted from [173] to illustrate the beam-steering concept under different bias states.

In [174], a metasurface-based reconfigurable antenna employing PIN diodes as the tuning mechanism is demonstrated for electrically controlled beam steering. As illustrated in Figure 5a, each unit cell integrates a PIN diode and biasing vias, enabling discrete switching between different reflection-phase states. In addition to PIN-diode switching, the metasurface employs two geometrically distinct unit-cell designs with different physical dimensions. Combining PIN-diode switching with two unit-cell geometries yields four discrete phase states, realizing a quasi-2-bit coding scheme. The metasurface module is constructed by spatially arranging the two unit-cell types, enabling expanded phase coverage. The corresponding phase distributions are shown in Figure 5b,c, where different digital coding states produce beam steering toward $\theta = -18^\circ$ and $\theta = 18^\circ$. This hybrid approach enables multi-state phase control through a compact unit-cell configuration with minimal biasing complexity.

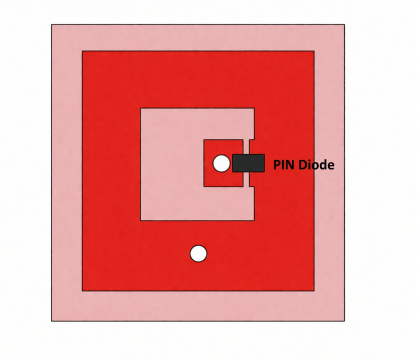

(**a**)

Figure 5. *Cont.*

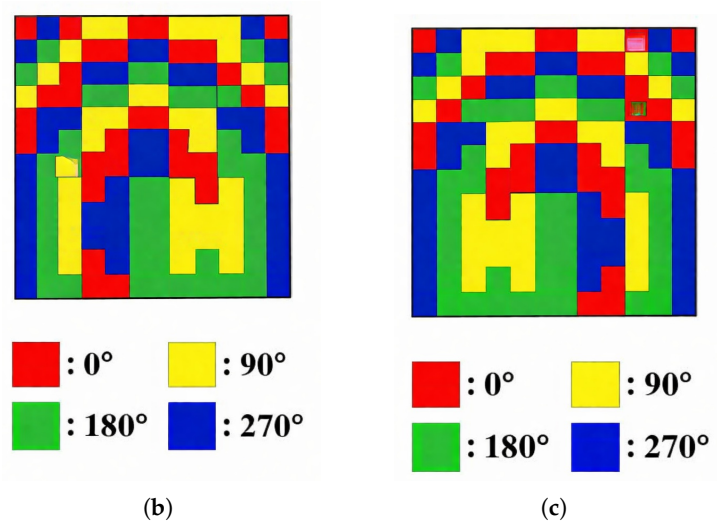

(**b**) (**c**)

Figure 5. Quasi-2-bit metasurface antenna. (**a**) Geometry of the reconfigurable unit cell with integrated PIN diode adapted from [174]. (**b**,**c**) Representativephase distributions of the metasurface corresponding to two considered beam-steering states, showing four discrete phase levels (0°, 90°, 180°, and 270°) adapted from [174].

4.2. Polarization Reconfiguration

Polarization reconfiguration is another important application of tunable metasurfaces in antenna and electromagnetic systems. By dynamically adjusting the response of metasurface unit cells, such structures enable real-time control over the polarization state of radiated or reflected waves, including switching between linear, circular, and elliptical polarizations. This capability is particularly valuable in wireless communications, sensing, and imaging systems, where polarization diversity can improve link robustness, mitigate interference, and enhance system adaptability without requiring multiple antennas or mechanical reorientation.

In [175], an electrically reconfigurable polarization converter based on an active metasurface is presented for dynamic polarization control. The metasurface is composed of periodically arranged anisotropic unit cells loaded with PIN diodes, enabling polarization reconfiguration in the transmission mode. As illustrated in Figure 6a, the unit cell consists of elliptic split-ring elements arranged on a thin dielectric substrate, forming an active metasurface whose polarization response can be controlled through discrete bias states. By switching the bias state of the integrated PIN diodes, the metasurface enables polarization switching between linear and circular polarization for an incident linearly polarized wave oriented at 45° with respect to the metasurface axes.

The metasurface is subsequently integrated as a superstrate of a horn antenna to enable polarization reconfiguration of the antenna, as shown in Figure 6b. The antenna polarization can be reconfigured without modifying its structure, confirming the suitability of tunable metasurfaces for polarization-reconfigurable antenna systems.

In [176], a graphene-based metasurface is applied to realize a polarization-reconfigurable terahertz antenna. The metasurface functions as a polarization-conversion layer integrated with a dual-band antenna, enabling dynamic control of the antenna polarization state without altering the physical geometry. By electrically tuning the graphene layer, the antenna can switch between linearly polarized and circularly polarized radiation at two distinct terahertz frequency bands. The unit-cell configuration of the graphene polarization-conversion metasurface and the antenna layout are illustrated in Figure 7. The integration of the metasurface with the antenna is illustrated in Figure 8. The results confirm stable po-

larization switching with consistent radiation characteristics, highlighting the suitability of graphene-based metasurfaces for polarization reconfiguration in terahertz antenna systems.

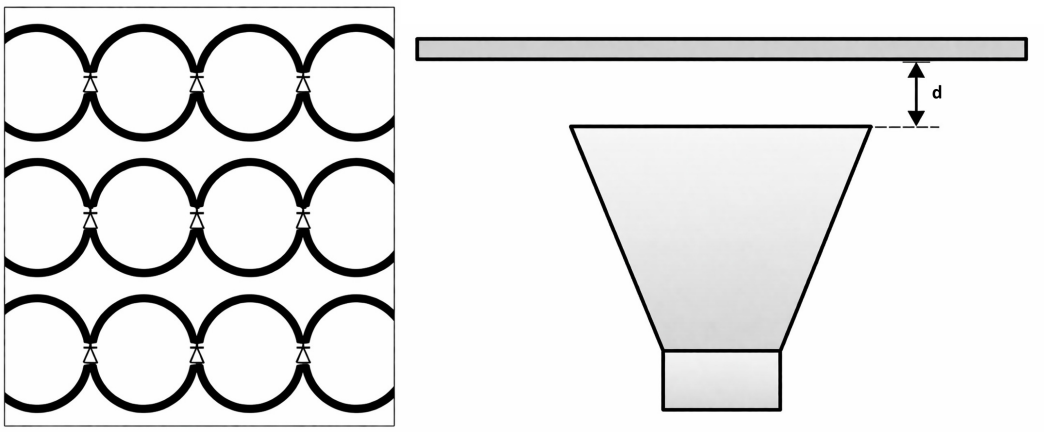

(**a**) (**b**)

Figure 6. (**a**) Unit-cell geometry of PIN-diode-controlled metasurface for polarization reconfiguration and (**b**) metasurface used as a superstrate above a horn antenna, both adapted from [175].

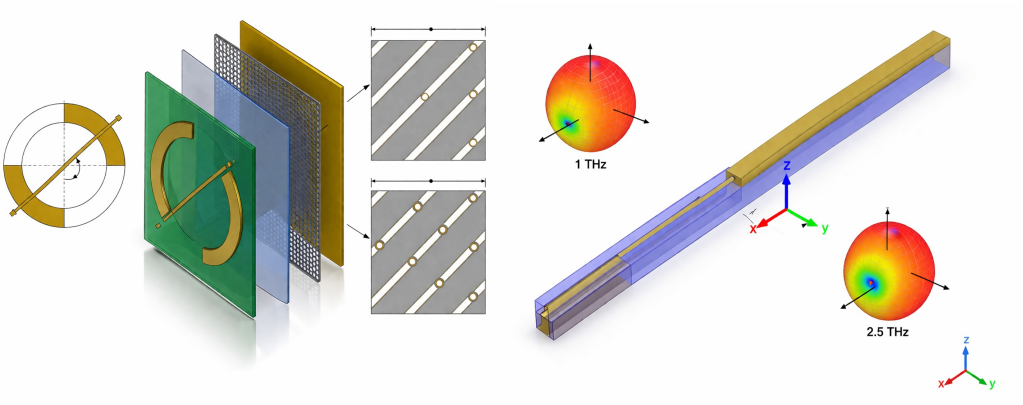

(**a**) (**b**)

Figure 7. (**a**) Layout of the metasurface unit cell; (**b**) Antenna structure and corresponding representativeradiation patterns at different operating frequencies, both adapted from [176].

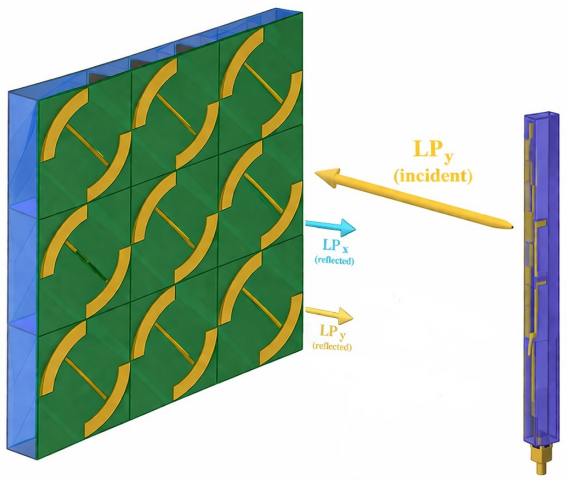

Figure 8. The integration of the metasurface with the antenna, adapted from [176].

4.3. Frequency Reconfiguration and Multiband Operation

Frequency reconfiguration represents another key application of tunable metasurfaces in reconfigurable antenna systems, enabling dynamic control of the operating frequency or the realization of multiband functionality within a single radiating aperture. By modifying the electromagnetic response of the metasurface unit cells through electrically or externally controlled tuning elements, the resonance frequency of the antenna can be adjusted without altering its physical geometry. This capability allows antennas to adapt to different frequency bands, support band switching, or achieve continuous frequency tuning, which is particularly desirable for modern wireless, sensing, and adaptive communication systems [59,177].

A frequency-reconfigurable metasurface antenna is presented in [11], realized by integrating a tunable metasurface layer incorporating vanadium dioxide (VO_2) films. The frequency agility is achieved by exploiting the reversible insulator-to-metal transition of VO_2, which induces a substantial change in the electromagnetic response of the metasurface. As a result, the antenna operates at two distinct frequency bands corresponding to the dielectric and metallic states of VO_2, without modifying the antenna geometry or feeding network.

Figure 9a shows the geometry of the proposed metasurface unit cell. As illustrated, the VO_2 film is placed across the branch gap within the metasurface unit cell, making the unit-cell response dependent on the material state of VO_2. In the semiconducting state, the high resistivity of VO_2 results in a weak electrical coupling across the gap, while in the metallic state, the reduced resistivity enhances the coupling between the branches. The change in unit-cell behavior is attributed to the large variation in the electrical properties of VO_2 during the insulator-to-metal transition, as expressed by an equivalent circuit model in the paper. The corresponding antenna performance is summarized in Figure 9b. When the VO_2 film is in its insulating state, the antenna operates over the 23.25–24.3 GHz band with a maximum gain of approximately 8.7 dBi. Upon transition of VO_2 to the metallic state, the operating band shifts to 37–39.8 GHz, where a peak gain of about 7.6 dBi is achieved, confirming that the VO_2 phase transition provides a clear two-state frequency reconfiguration.

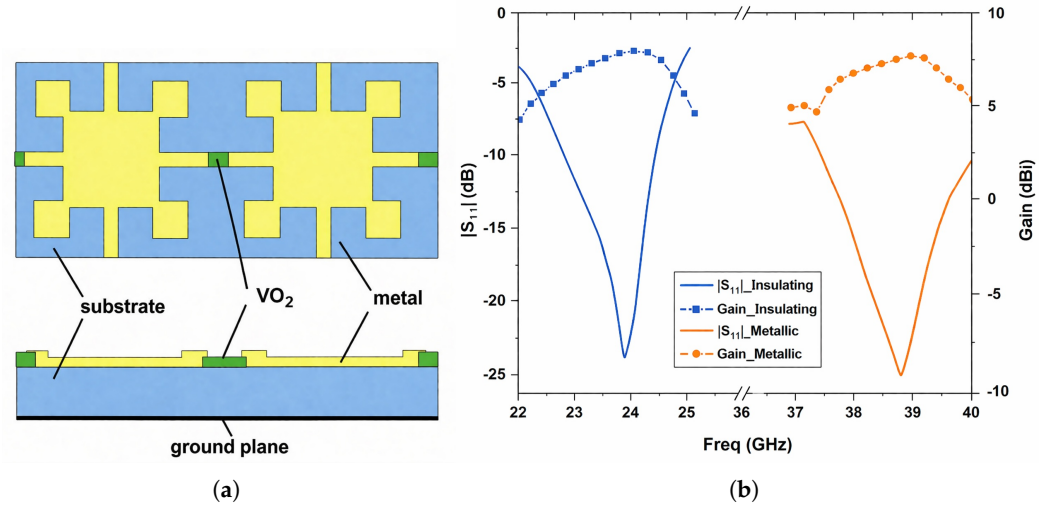

Figure 9. (**a**) Schematic of the VO_2-integrated metasurface unit cell, (**b**) Representative reflection coefficient and realized gain for the insulating and metallic states of VO_2, both adapted from [11].

In [114], a liquid-crystal-tunable metamaterial unit cell is introduced as an enabling element for frequency-reconfigurable metasurface antennas. By integrating a nematic LC layer into the metasurface structure, the effective dielectric properties of the unit cell can be

continuously adjusted through an external bias, leading to a shift in its resonant frequency. The results demonstrate a wide and stable frequency tuning range within a compact planar configuration, highlighting the potential of liquid-crystal-loaded metasurfaces for dynamic and frequency-agile antenna apertures.

4.4. Multifunctional Tunable Metasurface Antennas

Multifunctional antennas enabled by tunable metasurfaces provide the capability to dynamically switch between multiple operational modes within a single radiating structure. By exploiting the programmable electromagnetic response of metasurfaces, such antennas can support different combinations of frequency bands, radiation patterns, and polarization states without increasing system complexity or antenna size. This mode-switching functionality allows a single antenna platform to adapt to diverse operational requirements, making tunable metasurface-based designs particularly attractive for compact, adaptive, and next-generation wireless systems [178,179].

In [180,181], 1-bit reconfigurable transmit- and reflectarray antennas based on tunable metasurface architectures are reported. Each metasurface unit cell integrates PIN diodes that switch the electromagnetic response between two discrete states, enabling digital control of the aperture phase. By appropriately configuring the diode states across the surface, the antennas can dynamically operate in either transmitarray or reflectarray mode within the same physical structures. Figure 10 provides a conceptual illustration of the reconfigurable transmit–reflect metasurface antenna capable of independently manipulating reflected and transmitted waves to support users in different spatial regions [180].

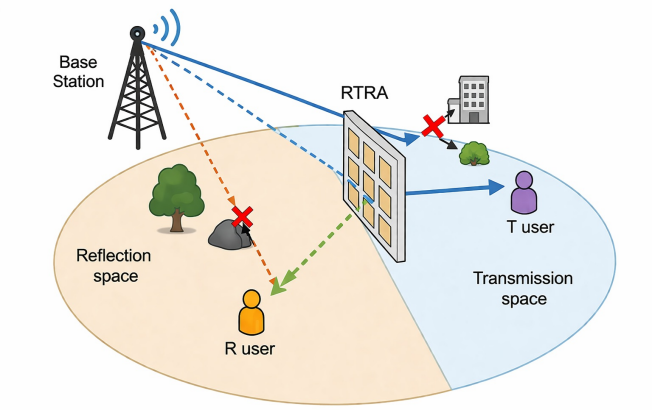

Figure 10. Conceptual illustration of the reconfigurable transmit–reflect metasurface design, adapted from [180].

In [182,183], multifunctional antenna operation is realized through radiation pattern reconfiguration enabled by PIN-diode-controlled programmable metasurface apertures. In both works, a single metasurface-based structure supports multiple radiation functions, including sum beams for directive radiation and difference beams for monopulse operation, with the ability to electronically switch between these modes. These beam patterns are synthesized by programming the phase distribution across the metasurface aperture, while a single feed antenna is used only as an illuminator. Reference [182] realizes this functionality using a reflective metasurface and [183] adapts this concept to a transmit array configuration, and both designs demonstrate that tunable metasurface apertures can integrate beam shaping, beam steering, and monopulse operation within a single antenna platform.

The metasurface unit cell integrating PIN diodes and biasing vias is illustrated in Figure 11, highlighting the multilayer configuration used to enable discrete phase control.

The corresponding measured and simulated radiation patterns in Figure 12a,b show clear formation of sum and difference beams in the E-plane, with good agreement between simulation and measurement. Beyond mode switching between sum and difference beams, the metasurface also supports electronic beam steering through reconfiguration of the coding patterns across the aperture.

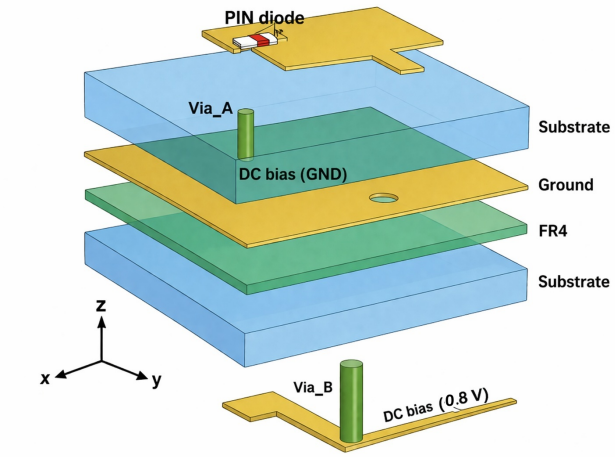

Figure 11. Geometry of the metasurface unit cell incorporating PIN diodes and biasing vias, adapted from [182].

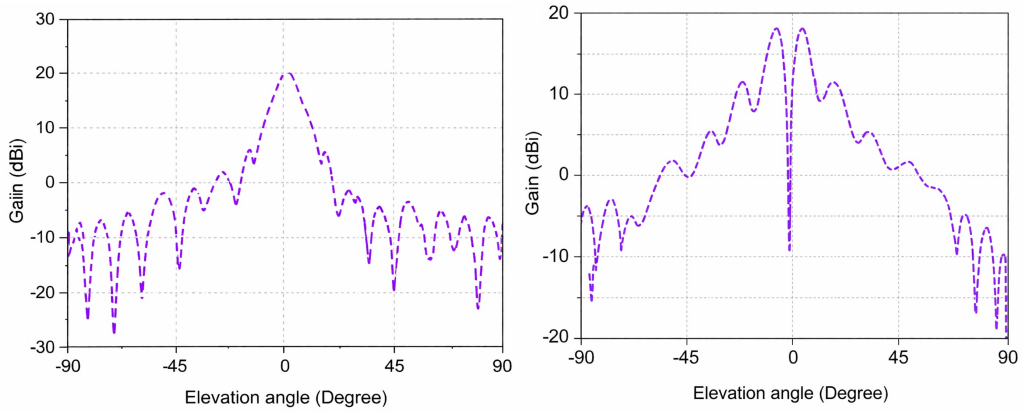

(**a**) (**b**)

Figure 12. RepresentativeE-plane radiation patterns of the metasurface antenna for (**a**) sum-beam and (**b**) difference-beam operation, both adapted from [182].

In [94], a multifunctional metasurface antenna is proposed that simultaneously enables beam steering, polarization conversion, and phase offset control within a single reflective aperture. Figure 13a illustrates the metasurface unit cell, which consists of a metallic pattern incorporating a varactor allowing reflection-phase control. By properly adjusting the spatial phase distribution across the metasurface, the reflected wavefront can be shaped while maintaining polarization control. Figure 13b presents the conceptual operation of the metasurface, demonstrating its ability to manipulate the propagation direction and polarization state of an incident wave using a single planar structure.

The multifunctional performance is experimentally validated through measured radiation patterns shown in Figure 14. These results demonstrate polarization-selective beam steering for multiple polarization states, including XP-to-XP, YP, left-hand circular polarization (LHCP), and right-hand circular polarization (RHCP) conversions, over a wide angular range. The metasurface achieves directive performance while switching between differ-

ent polarization responses, confirming that beam steering and polarization conversion are realized simultaneously.

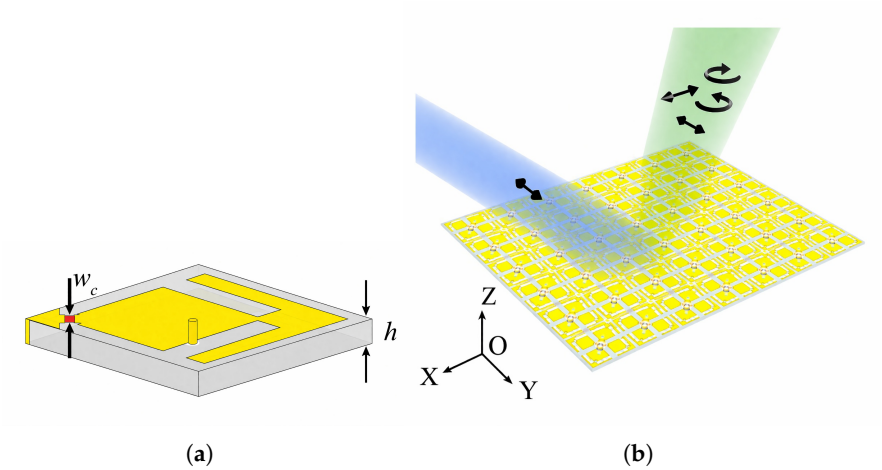

Figure 13. (**a**) Geometry of the metasurface unit cell with key structural parameters. (**b**) Perspective view of the metasurface aperture illustrating beam steering and polarization manipulation under different coding states, both adapted from [94].

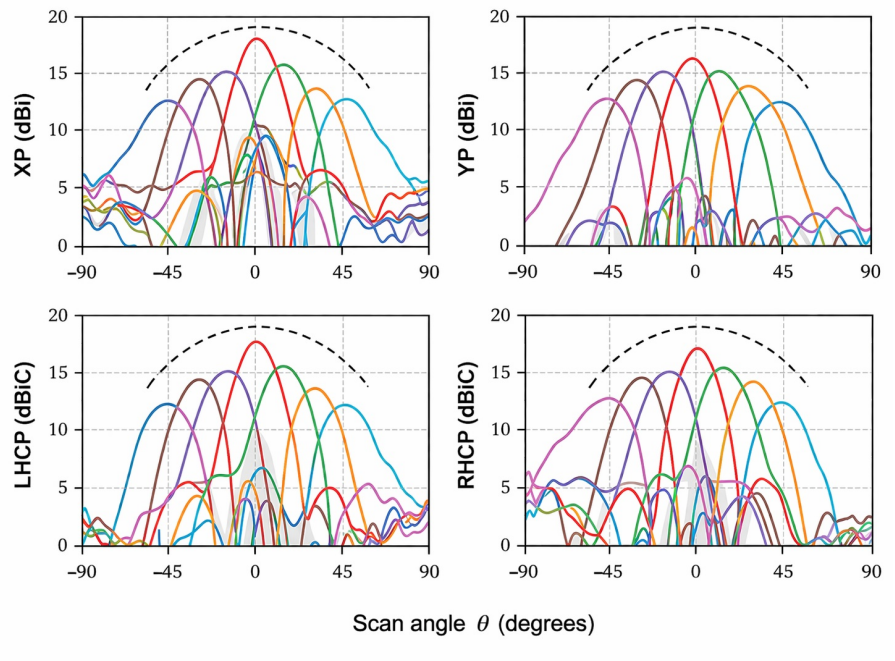

Figure 14. Representative radiation patterns demonstrating simultaneous beam steering and polarization control for different polarization states: XP-to-XP, YP, LHCP, and RHCP conversions, adapted from [94]. Different colored curves correspond to different steering angles.

5. Design Challenges and Future Perspectives of Tunable Metasurface Antennas

Despite the rapid progress in tunable metasurface antennas, several practical challenges remain before these systems can be widely adopted in next-generation wireless platforms. While various tuning mechanisms—including PIN diodes, varactors, RF-MEMS switches, LCs, phase-change materials (PCMs), and two-dimensional materials—enable dynamic control of electromagnetic responses, their integration into large-aperture, high-performance antenna systems introduces significant design trade-offs [11,184].

5.1. Design Challenges

A. Loss and Efficiency Degradation

One of the primary limitations of tunable metasurfaces is the additional loss introduced by active components. Semiconductor-based tuning elements such as PIN diodes and varactors introduce ohmic resistance and parasitic capacitance, which degrade radiation efficiency and reduce gain, particularly at millimeter-wave and terahertz frequencies [185,186]. Similarly, LCs exhibit dielectric loss at higher frequencies, while VO_2-based phase-change materials may suffer from increased absorption in their metallic state [184,187]. In large-aperture reflectarrays or transmitarrays, these losses accumulate across hundreds or thousands of unit cells, significantly impacting overall efficiency. RF-MEMS switches offer lower insertion loss compared to semiconductor devices; however, their low switching speed, packaging complexity, and fabrication cost remain concerns [11,188]. Therefore, achieving high radiation efficiency while maintaining reconfigurability remains a major design challenge.

In metasurface-based antennas, these losses are further amplified due to the distributed nature of the aperture. Since the overall radiation performance results from the collective response of a large number of unit cells, even small losses at the unit-cell level can accumulate and significantly reduce the aperture efficiency. In addition, phase tuning is inherently associated with changes in the unit-cell impedance and resonance condition, which simultaneously affect both amplitude and phase responses. As a result, unit cells designed to provide specific phase shifts may also exhibit different amplitude levels. While the required phase variation across the metasurface is preserved, the accompanying amplitude nonuniformity alters the relative contribution of individual unit cells in the overall field superposition. This leads to distortions in the resulting wavefront, degrading beamforming accuracy and increasing sidelobe levels.

B. Biasing Network Complexity and Electromagnetic Interference

In tunable metasurface antennas, reconfiguration is typically realized by applying external control signals such as DC bias voltages, electric or magnetic fields, temperature variations, mechanical stress, or optical excitation. These control inputs modify the electrical properties of the unit cells and consequently alter the electromagnetic response of the metasurface. However, achieving adaptive functionality generally requires dedicated biasing networks and additional circuit components. The presence of bias lines, vias, capacitors, and inductors increases structural complexity and can degrade RF performance. In densely packed arrays, these additional elements may introduce parasitic coupling, insertion loss, impedance perturbations, and distortion of the radiation characteristics. Furthermore, the associated control hardware increases power consumption and limits scalability to large apertures, motivating ongoing research toward minimizing the electromagnetic impact of bias circuitry in metasurface-based antennas [185,189]. This challenge becomes particularly critical in large-scale and high-frequency implementations, where the bias network directly influences overall antenna performance.

In large-scale metasurface apertures consisting of hundreds or thousands of unit cells, the biasing network must be treated as an integral part of the electromagnetic design rather than a purely electrical subsystem. The routing of bias lines across the aperture introduces parasitic radiation, phase perturbations, and mutual coupling between adjacent unit cells, which can significantly affect the intended wavefront manipulation.

A key challenge arises from the fact that bias lines and vias may behave as unintended radiating elements, especially when their physical dimensions become comparable to a fraction of the operating wavelength. This effect is particularly pronounced at millimeter-wave and terahertz frequencies, where even short interconnects can disturb the local

electromagnetic response. As a result, improper routing can degrade beamforming accuracy, increase sidelobe levels, and distort the desired phase distribution across the metasurface. Moreover, in densely packed arrays, the proximity of control lines can lead to strong electromagnetic coupling between neighboring elements, reducing the independence of unit-cell tuning and complicating precise phase control in beam-steering and wavefront-shaping applications.

Although the biasing network can noticeably affect aperture efficiency and sidelobe levels in dense arrays, its impact is strongly design-dependent and is rarely reported as a separate figure of merit; instead, it is usually embedded in the measured overall array efficiency and radiation pattern.

To address electromagnetic interference introduced by biasing networks in large-scale metasurface arrays, detailed routing and isolation strategies must be carefully implemented at both the unit-cell and system levels. In particular, bias lines can act as unintended radiating elements or scattering paths if they carry RF currents, thereby disturbing the designed current distribution on the metasurface. To suppress this effect, DC and RF paths are typically separated using high-impedance bias lines or RF chokes, which prevent RF signals from propagating along the control network while allowing the required biasing signals to pass. Additionally, resistive or distributed biasing grids are employed to damp parasitic currents and reduce the formation of standing waves along bias lines.

From a layout perspective, routing bias traces along regions of minimal surface current or electromagnetic field intensity is essential to limit their interaction with the radiating elements. This is particularly important in large apertures, where dense routing networks can otherwise introduce significant coupling and unintended scattering. Multilayer configurations further improve isolation by relocating bias networks to separate layers, with vertical interconnects (vias) providing localized connections to the unit cells while minimizing disruption to the radiating surface. Grounded shielding layers and proper grounding schemes can also be incorporated to reduce electromagnetic leakage and coupling between control and RF signals.

Moreover, symmetric and periodic routing strategies are often adopted to maintain uniform electromagnetic behavior across the metasurface and avoid pattern distortion caused by asymmetric bias layouts. These combined approaches demonstrate that effective co-design of the biasing network and metasurface geometry is essential for preserving radiation efficiency, minimizing parasitic effects, and enabling scalable implementation of large-scale reconfigurable metasurface antennas [91,190–192].

C. Switching Speed

The dynamic response of tunable metasurfaces is primarily determined by the underlying physical tuning mechanism. Semiconductor devices such as PIN diodes offer nanosecond-scale switching speeds, making them suitable for high-speed beam steering, adaptive communication links, and real-time reconfigurable systems. Varactor diodes provide continuous tuning with similarly fast intrinsic electrical response, although the effective switching time may be influenced by bias-network time constants and control circuitry. Multiple-input multiple-output (MIMO) switches typically exhibit microsecond-scale switching times, determined by the mechanical motion of the movable membrane. Material-based tuning mechanisms generally operate at slower time scales. LCs rely on molecular reorientation under an applied electric field and typically respond in milliseconds. Thermal phase-change materials such as VO_2 can exhibit microsecond-to-millisecond switching depending on the excitation mechanism, whereas optically or electrically driven phase transitions may achieve faster response at the expense of increased power consumption.

From a system perspective, switching speed directly impacts the feasibility of beam tracking, adaptive MIMO systems, frequency hopping, and RIS applications. Consequently,

the choice of tuning mechanism involves a trade-off between response time, insertion loss, tuning range, power consumption, and implementation complexity [103,193–197].

D. Practical Limitations and Industrial Considerations

Beyond the primary challenges, several additional practical limitations affect tunable metasurface antennas. Nonlinear behavior of semiconductor-based tuning elements may degrade spectral purity and dynamic range under high RF power [198,199]. Fabrication tolerances and component variability can introduce phase errors across electrically large apertures, reducing beamforming accuracy and increasing sidelobe levels. In practical environments, thermal effects, particularly under varying or extreme temperature conditions, can lead to performance drift by altering material properties and biasing conditions [200,201]. In addition, long-term reliability and lifetime performance under repeated switching operations remain critical concerns, as device degradation and variability may accumulate over time [202–204]. From a manufacturing perspective, achieving consistent and reproducible performance across large-area metasurfaces is challenging due to material inhomogeneity, process variations, and the complexity of integrating large-scale biasing networks. Moreover, large-scale integration of tunable materials or active components into standard PCB and integrated fabrication processes remains technologically demanding [185,186,205,206]. These factors highlight important engineering reliability challenges that must be addressed for practical and industrial deployment.

5.2. Intelligent Control and Machine Learning for Large-Scale Metasurfaces

An important emerging direction in tunable metasurface antennas is their evolution toward programmable information metasurfaces and reconfigurable intelligent surfaces (RISs). In these systems, large arrays with hundreds or thousands of unit cells must be controlled in real time. Conventional tuning methods become inefficient in this context due to the large number of control parameters and the coupling between unit cells. As a result, data-driven and machine-learning-based approaches have attracted increasing attention [207,208].

Machine learning provides an effective framework for optimizing metasurface configurations under complex and dynamic conditions. For instance, codebook-based methods can be combined with learning techniques to reduce the search space and enable fast beam selection and adaptive beamforming. Reinforcement learning has also been investigated to learn control strategies without relying on explicit electromagnetic models, making it suitable for time-varying or uncertain environments [209,210].

In addition, supervised and deep learning models have been used to directly map desired electromagnetic responses, such as beam direction, polarization, or frequency, to the corresponding metasurface configurations. This significantly reduces the need for computationally intensive full-wave optimization and enables real-time operation. Furthermore, machine-learning-assisted beam-search algorithms can reduce control latency by quickly identifying near-optimal configurations with limited feedback [211,212].

Despite these advantages, several challenges remain unresolved. These include the need for large training datasets, reduced performance under varying operating conditions, and practical hardware constraints such as limited phase resolution due to discrete tuning states. Future research directions include the development of more data-efficient learning methods, improved adaptability in dynamic environments, and the co-design of electromagnetic structures and intelligent control algorithms. In addition, the development of scalable real-time control strategies and efficient hardware implementations will be essential for enabling practical large-scale metasurface systems [207,213–218].

6. Conclusions

This review presents a comprehensive overview of tunable metasurface antennas, with emphasis on underlying tuning mechanisms, implementation strategies, and emerging applications in radiation pattern reconfiguration, polarization control, frequency agility, and multifunctional operation. Various reconfiguration approaches, including semiconductor switches (PIN diodes and varactors), RF-MEMS devices, LCs, phase-change materials, and two-dimensional materials, were investigated in terms of their physical principles, performance trade-offs, switching characteristics, and integration complexity.

Application-oriented discussions highlighted how tunable metasurfaces enable dynamic beam steering, polarization switching, frequency reconfiguration, and simultaneous multifunction radiation control within compact and planar antenna platforms. Practical challenges associated with biasing networks, switching speed, fabrication tolerances, scalability, and material integration were also analyzed. These factors are essential to ensure that initial prototype designs can be successfully developed into reliable large-area systems capable of operating at high frequencies and under high power conditions.

Overall, tunable metasurface antennas represent a promising paradigm for next-generation adaptive electromagnetic systems. Continued advancements in material engineering, device integration, and large-scale programmable architectures are expected to further expand their capabilities and facilitate their deployment in future communication, sensing, and radar technologies.

Funding: This research received no external funding.

Data Availability Statement: The paper is a review and no new data were created.

Conflicts of Interest: The authors declare no conflicts of interest.

References

1. Subbaraj, S.; Thomas, S.B. Reconfigurable antennas and their practical applications—A review. *Radio Sci.* **2023**, *58*, e2023RS007656. [CrossRef]
2. Suryapaga, V.; Khairnar, V.V. Review on Multifunctional Pattern and Polarization Reconfigurable Antennas. *IEEE Access* **2024**, *12*, 90218–90251. [CrossRef]
3. Fallahpour, M.; Ghasr, M.T.; Zoughi, R. Miniaturized Reconfigurable Multiband Antenna For Multiradio Wireless Communication. *IEEE Trans. Antennas Propag.* **2014**, *62*, 6049–6059. [CrossRef]
4. García, E.; Andújar, A.; Anguera, J. Overview of Reconfigurable Antenna Systems for IoT Devices. *Electronics* **2024**, *13*, 3988. [CrossRef]
5. Gianvittorio, J.P.; Rahmat-Samii, Y. Reconfigurable Patch Antennas Using Switchable Slots for Circular Polarization Diversity. *IEEE Trans. Antennas Propag.* **2005**, *53*, 3567–3574.
6. Ojaroudi Parchin, N.; Jahanbakhsh Basherlou, H.; Al-Yasir, Y.I.A.; Abdulkhaleq, A.M.; Abd-Alhameed, R.A. Reconfigurable Antennas: Switching Techniques—A Survey. *Electronics* **2020**, *9*, 336. [CrossRef]
7. Karthika, K.; Kavitha, K. Reconfigurable Antennas for Advanced Wireless Communications: A Review. *Wirel. Pers. Commun.* **2021**, *118*, 2711–2771. [CrossRef]
8. Mittra, R.; Chan, C.; Cwik, T. Techniques for analyzing frequency selective surfaces—A review. *Proc. IEEE* **1988**, *76*, 1593–1615. [CrossRef]
9. Yang, W.; Li, J.; Chen, D.; Cao, Y.; Xue, Q.; Che, W. Advanced Metasurface-Based Antennas: A Review. *IEEE Open J. Antennas Propag.* **2025**, *6*, 6–24. [CrossRef]
10. Yang, W.; Che, W.; Jin, H.; Feng, W.; Xue, Q. A Polarization-Reconfigurable Dipole Antenna Using Polarization Rotation AMC Structure. *IEEE Trans. Antennas Propag.* **2015**, *63*, 5305–5315. [CrossRef]
11. Yang, W.; Zhou, C.; Xue, Q.; Wen, Q.; Che, W. Millimeter-Wave Frequency-Reconfigurable Metasurface Antenna Based on Vanadium Dioxide Films. *IEEE Trans. Antennas Propag.* **2021**, *69*, 4359–4369. [CrossRef]
12. Barbuto, M.; Hamzavi-Zarghani, Z.; Longhi, M.; Monti, A.; Ramaccia, D.; Vellucci, S.; Toscano, A.; Bilotti, F. Metasurfaces 3.0: A New Paradigm for Enabling Smart Electromagnetic Environments. *IEEE Trans. Antennas Propag.* **2022**, *70*, 8883–8897. [CrossRef]

13. Vellucci, S.; Monti, A.; Barbuto, M.; Hamzavi-Zarghani, Z.; Longhi, M.; Ramaccia, D.; Stefanini, L.; Toscano, A.; Bilotti, F. Metasurface Coatings Enabling Antenna Reconfigurability for Next-generation Communications Smart Repeaters. In Proceedings of the 2023 Seventeenth International Congress on Artificial Materials for Novel Wave Phenomena (Metamaterials), Chania, Greece, 11–14 September 2023; pp. X-405–X-407. [CrossRef]
14. Hamzavi-Zarghani, Z.; Yahaghi, A.; Matekovits, L. Reconfigurable metasurface lens based on graphene split ring resonators using Pancharatnam–Berry phase manipulation. *J. Electromagn. Waves Appl.* **2019**, *33*, 572–583. [CrossRef]
15. Schennum, G.H. Frequency-Selective Surfaces for Multiple-Frequency Antennas. *Microw. J.* **1973**, *16*, 55–57.
16. Tsao, C.H.; Mittra, R. Spectral-domain analysis of frequency selective surfaces comprised of periodic arrays of cross dipoles and Jerusalem crosses. *IEEE Trans. Antennas Propag.* **1984**, *32*, 478–486. [CrossRef]
17. Zhang, W.; Song, H. Analysis of Mechanically Tunable Frequency Selective Surfaces. *J. Syst. Eng. Electron.* **1997**, *8*, 7–16.
18. Sievenpiper, D.; Zhang, L.; Broas, R.; Alexopolous, N.; Yablonovitch, E. High-impedance electromagnetic surfaces with a forbidden frequency band. *IEEE Trans. Microw. Theory Tech.* **1999**, *47*, 2059–2074. [CrossRef]
19. Barnes, W.L.; Priest, T.W.; Kitson, S.C.; Sambles, J.R. Physical origin of photonic energy gaps in the propagation of surface plasmons on gratings. *Phys. Rev. B* **1996**, *54*, 6227–6244. [CrossRef]
20. Kitson, S.C.; Barnes, W.L.; Sambles, J.R. Full photonic band gap for surface modes in the visible. *Phys. Rev. Lett.* **1996**, *77*, 2670–2673. [CrossRef]
21. De Sabata, A.; Matekovits, L. Unit-Cell Geometry in Stripline Technology Featuring Sequential Band-Gaps Between Every Two Consecutive Modes. *IEEE Antennas Wirel. Propag. Lett.* **2012**, *11*, 97–100. [CrossRef]
22. de Maagt, P.; Gonzalo, R.; Vardaxoglou, J.; Baracco, J.M. Review of electromagnetic-bandgap technology and applications. *URSI Radio Sci. Bull.* **2004**, *2004*, 11–25 .
23. Vosoogh, A.; Kildal, P.S. Corporate-Fed Planar 60-GHz Slot Array Made of Three Unconnected Metal Layers Using AMC Pin Surface for the Gap Waveguide. *IEEE Antennas Wirel. Propag. Lett.* **2016**, *15*, 1935–1938. [CrossRef]
24. Yu, N.; Genevet, P.; Kats, M.A.; Aieta, F.; Tetienne, J.P.; Capasso, F.; Gaburro, Z. Light propagation with phase discontinuities: Generalized laws of reflection and refraction. *Science* **2011**, *334*, 333–337. [CrossRef] [PubMed]
25. Sun, S.; He, Q.; Xiao, S.; Xu, Q.; Li, X.; Zhou, L. Gradient-index meta-surfaces as a bridge linking propagating waves and surface waves. *Nat. Mater.* **2012**, *11*, 426–431. [CrossRef]
26. Ni, X.; Emani, N.K.; Kildishev, A.V.; Boltasseva, A.; Shalaev, V.M. Broadband light bending with plasmonic nanoantennas. *Science* **2012**, *335*, 427. [CrossRef] [PubMed]
27. Kildishev, A.V.; Boltasseva, A.; Shalaev, V.M. Planar photonics with metasurfaces. *Science* **2013**, *339*, 1232009. [CrossRef]
28. Holloway, C.L.; Kuester, E.F.; Gordon, J.A.; O'Hara, J.; Booth, J.; Smith, D.R. An Overview of the Theory and Applications of Metasurfaces: The Two-Dimensional Equivalents of Metamaterials. *IEEE Antennas Propag. Mag.* **2012**, *54*, 10–35. [CrossRef]
29. Glybovski, S.B.; Tretyakov, S.A.; Belov, P.A.; Kivshar, Y.S.; Simovski, C.R. Metasurfaces: From microwaves to visible. *Phys. Rep.* **2016**, *634*, 1–72. [CrossRef]
30. Alu, A.; Engheta, N. Tuning the scattering response of optical nanoantennas with nanocircuit loads. *Nat. Photonics* **2008**, *2*, 307–310. [CrossRef]
31. Chen, P.Y.; Alù, A. Mantle cloaking using thin patterned metasurfaces. *Phys. Rev. B* **2011**, *84*, 205110. [CrossRef]
32. Matekovits, L.; Bird, T.S. Width-Modulated Microstrip-Line Based Mantle Cloaks for Thin Single- and Multiple Cylinders. *IEEE Trans. Antennas Propag.* **2014**, *62*, 2606–2615. [CrossRef]
33. Soric, J.C.; Monti, A.; Toscano, A.; Bilotti, F.; Alù, A. Multiband and Wideband Bilayer Mantle Cloaks. *IEEE Trans. Antennas Propag.* **2015**, *63*, 3235–3240. [CrossRef]
34. Younesiraad, H.; Hamzavi-Zarghani, Z.; Matekovits, L. Invisibility Utilizing Huygens' Metasurface Based on Mantle Cloak and Scattering Suppression Phenomen. *IEEE Trans. Antennas Propag.* **2021**, *69*, 5181–5186. [CrossRef]
35. Hosseini, K.; Younesiraad, H.; Monti, A.; Toscano, A.; Bilotti, F. Low-Profile Dual-Band and Wideband Optical Mantle Cloaks with Electric and Magnetic Polarizabilities and High Scattering Efficiency. *IEEE Access* **2025**, *13*, 120244–120256. [CrossRef]
36. Pfeiffer, C.; Grbic, A. Metamaterial Huygens' Surfaces: Tailoring Wave Fronts with Reflectionless Sheets. *Phys. Rev. Lett.* **2013**, *110*, 197401. [CrossRef] [PubMed]
37. Ataloglou, V.G.; Eleftheriades, G.V. Arbitrary Wave Transformations with Huygens' Metasurfaces Through Surface-Wave Optimization. *IEEE Antennas Wirel. Propag. Lett.* **2021**, *20*, 1750–1754. [CrossRef]
38. Alù, A.; Maci, S.; Engheta, N. Metasurfaces and Metamaterials for Electromagnetics. *IEEE Trans. Antennas Propag.* **2025.** [CrossRef]
39. Rauf, H.; Kamal, B.; Ullah, S.; Ali, U.; Matekovits, L. Experimental Validation of a Multi-Functional Metasurface for 5G and Satellite Communication. *IEEE Access* **2025**, *13*, 55476–55486. [CrossRef]
40. Ali, U.; Ullah, S.; Basir, A.; Yan, S.; Ren, H.; Kamal, B.; Matekovits, L. Design and performance investigation of metamaterial-inspired dual band antenna for WBAN applications. *PLoS ONE* **2024**, *19*, e0306737. [CrossRef]

41. Hamzavi-Zarghani, Z.; Monti, A.; Vellucci, S.; Barbuto, M.; Longhi, M.; Ramaccia, D.; Stefanini, L.; Toscano, A.; Bilotti, F. Overcoming limitations of passive invisible antennas through bianisotropic nonreciprocal mantle cloaks. *Phys. Rev. Appl.* **2024**, *21*, 064045. [CrossRef]
42. Hossain, A.; Pancrazio, S.; Kelley, T.; Pham, A.V. A Compact and Low-Profile High-Gain Multilayer Vivaldi Antenna Based on Gradient Metasurface Superstrates. *IEEE Antennas Wirel. Propag. Lett.* **2025**, *24*, 1537–1541. [CrossRef]
43. Bo, X.Z.; Yuan, B.W.; Tong, Y.X.; Liu, Z.G.; Cao, W.Q.; Shen, M. An Ultralow-Profile High-Gain Dual-Band Dual-Circularly Polarized Shared-Aperture Folded Transmitarray with Extremely Simple Structure. *IEEE Antennas Wirel. Propag. Lett.* **2026**, *25*, 259–263. [CrossRef]
44. Banting, H.A.; Saavedra, C.E. Bandwidth Enhancement of Low-Profile Metasurface Antenna Using Nonuniform Geometries. *IEEE Open J. Antennas Propag.* **2023**, *4*, 581–587. [CrossRef]
45. Wu, Z.; Li, L.; Li, Y.; Chen, X. Metasurface Superstrate Antenna with Wideband Circular Polarization for Satellite Communication Application. *IEEE Antennas Wirel. Propag. Lett.* **2016**, *15*, 374–377. [CrossRef]
46. Liu, W.; Chen, Z.N.; Qing, X. Metamaterial-Based Low-Profile Broadband Aperture-Coupled Grid-Slotted Patch Antenna. *IEEE Trans. Antennas Propag.* **2015**, *63*, 3325–3329. [CrossRef]
47. Liu, W.; Chen, Z.N.; Qing, X. Metamaterial-Based Low-Profile Broadband Mushroom Antenna. *IEEE Trans. Antennas Propag.* **2014**, *62*, 1165–1172. [CrossRef]
48. Yashchyshyn, Y.; Tokarsky, P. Using a metasurface to enhance the radiation efficiency of subterahertz antennas printed on thick substrates. *Sci. Rep.* **2024**, *14*, 18167. [CrossRef] [PubMed]
49. Alibakhshikenari, M.; Virdee, B.S.; See, C.H.; Abd-Alhameed, R.A.; Falcone, F.; Limiti, E. Surface wave reduction in antenna arrays using metasurface inclusion for MIMO and SAR systems. *Radio Sci.* **2019**, *54*, 1067–1075. [CrossRef]
50. Mu, W.; Xu, G.; Zhu, L.; Cao, Q. A Low-Profile Circularly Polarized Metasurface Antenna with RCS Reduction Enhanced by L-Shaped Branches. *IEEE Antennas Wirel. Propag. Lett.* **2026**, *25*, 339–343. [CrossRef]
51. Soric, J.C.; Monti, A.; Toscano, A.; Bilotti, F.; Alù, A. Dual-Polarized Reduction of Dipole Antenna Blockage Using Mantle Cloaks. *IEEE Trans. Antennas Propag.* **2015**, *63*, 4827–4834. [CrossRef]
52. Chen, D.; Yang, W.; Xue, Q.; Che, W. Miniaturized Wideband Planar Antenna Using Interembedded Metasurface Structure. *IEEE Trans. Antennas Propag.* **2021**, *69*, 3021–3026. [CrossRef]
53. Chen, D.; Xue, Q.; Yang, W.; Chin, K.S.; Jin, H.; Che, W. A Compact Wideband Low-Profile Metasurface Antenna Loaded with Patch-Via-Wall Structure. *IEEE Antennas Wirel. Propag. Lett.* **2023**, *22*, 179–183. [CrossRef]
54. Hamzavi-Zarghani, Z.; Atlasbaf, Z. A New Broadband Single-Layer Dual-Band Reflectarray Antenna in X- and Ku-Bands. *IEEE Antennas Wirel. Propag. Lett.* **2015**, *14*, 602–605. [CrossRef]
55. Longhi, M.; Vellucci, S.; Barbuto, M.; Monti, A.; Hamzavi-Zarghani, Z.; Stefanini, L.; Ramaccia, D.; Bilotti, F.; Toscano, A. Array Synthesis of Circular Huygens Metasurfaces for Antenna Beam-Shaping. *IEEE Antennas Wirel. Propag. Lett.* **2023**, *22*, 2649–2653. [CrossRef]
56. Monti, A.; Vellucci, S.; Longhi, M.; Barbuto, M.; Karamirad, M.; Hamzavi-Zarghani, Z.; Ramaccia, D.; Stefanini, L.; Toscano, A.; Bilotti, F. Static and Reconfigurable Phase-Gradient Metasurfaces for Antenna Applications. In Proceedings of the 2024 18th European Conference on Antennas and Propagation (EuCAP), Glasgow, UK, 17–22 March 2024; pp. 1–3. [CrossRef]
57. Wen, Y.; Qin, P.Y.; Maci, S.; Guo, Y.J. Low-Profile Multibeam Antenna Based on Modulated Metasurface. *IEEE Trans. Antennas Propag.* **2023**, *71*, 6568–6578. [CrossRef]
58. Rezaee, B.; Zarghani, Z.H.; Bösch, W. Design and Implementation of a Planar Lens Antenna Based on a Gradient-Index Metasurface. In Proceedings of the 2024 IEEE International Symposium on Antennas and Propagation and INC/USNC-URSI Radio Science Meeting (AP-S/INC-USNC-URSI), Florence, Italy, 14–19 July 2024; pp. 321–322. [CrossRef]
59. Hussain, M.; Awan, W.A.; Alzaidi, M.S.; Hussain, N.; Ali, E.M.; Falcone, F. Metamaterials and Their Application in the Performance Enhancement of Reconfigurable Antennas: A Review. *Micromachines* **2023**, *14*, 349. [CrossRef] [PubMed]
60. Ding, Z.; Li, J.; Cao, J.; Wang, H.; Chia, M.Y.W.; Nasimuddin, N. Wideband Dual-Polarized Metasurface Antenna with Polarization Reconfigurable Controlled by Diode and Resistor, Featuring Low RCS. *IEEE Antennas Wirel. Propag. Lett.* **2025**, *24*, 1208–1212. [CrossRef]
61. Chen, Y.; Wang, L.; Li, Z.; Li, Z.; Chen, J.; Bai, X.; Jin, R. Ka-Band Cross-Shaped Reconfigurable Metasurface Antenna for Agile Beam Modulation. *IEEE Trans. Antennas Propag.* **2025**, *73*, 6127–6132. [CrossRef]
62. Nam, Y.H.; Lee, J.H. A High-Efficiency Quasi-4-bit Reconfigurable Metasurface Antenna for Continuous Beam Steering with a Simple Bias Circuit. *IEEE Trans. Antennas Propag.* **2025**, *73*, 8248–8252. [CrossRef]
63. Ji, L.Y.; Han, Y.; Hong, X. Low-RCS Frequency-Reconfigurable Fabry–Perot Antenna Based on Liquid Metal Metasurface. *IEEE Antennas Wirel. Propag. Lett.* **2025**, *24*, 4417–4421. [CrossRef]
64. Lu, Y.; Zhang, S.; Li, L.; Han, J.; Ma, X.; Ma, S.; Shi, G. A Dual-Mode Reconfigurable Reflective Metasurface Element for Modulation and Detection. *IEEE Antennas Wirel. Propag. Lett.* **2026**, *25*, 359–363. [CrossRef]

65. Barbuto, M.; Hamzavi-Zarghani, Z.; Longhi, M.; Marini, A.V.; Monti, A.; Ramaccia, D.; Vellucci, S.; Toscano, A.; Bilotti, F. Intelligence Enabled by 2D Metastructures in Antennas and Wireless Propagation Systems. *IEEE Open J. Antennas Propag.* **2022**, *3*, 135–153. [CrossRef]
66. Wang, Z.; Huang, Y.; Liu, W.; Wang, H.M. Anti-Jamming Sensing with Distributed Reconfigurable Intelligent Metasurface Antennas. *IEEE Trans. Wirel. Commun.* **2026**, *25*, 6681–6694. [CrossRef]
67. Wei, X.; Wang, H.M. Multi-User Downlink with Reconfigurable Intelligent Metasurface Antennas (RIMSA) Array. *IEEE Trans. Veh. Technol.* **2025**, *74*, 18914–18929. [CrossRef]
68. Shi, H.; Li, J.; Zhang, A.; Jiang, Y.; Wang, J.; Xu, Z.; Xia, S. Gradient Metasurface with Both Polarization-Controlled Directional Surface Wave Coupling and Anomalous Reflection. *IEEE Antennas Wirel. Propag. Lett.* **2015**, *14*, 104–107. [CrossRef]
69. Forouzmand, A.; Tao, S.; Jafar-Zanjani, S.; Cheng, J.; Salary, M.M.; Mosallaei, H. Double split-loop resonators as building blocks of metasurfaces for light manipulation: Bending, focusing, and flat-top generation. *J. Opt. Soc. Am. B* **2016**, *33*, 1411–1420. [CrossRef]
70. Khajeh, A.; Hamzavi-Zarghani, Z.; Yahaghi, A.; Farmani, A. Tunable broadband polarization converters based on coded graphene metasurfaces. *Sci. Rep.* **2021**, *11*, 1296. [CrossRef] [PubMed]
71. Hamzavi-Zarghani, Z.; Yahaghi, A.; Matekovits, L. Dynamically Tunable Scattering Manipulation of Dielectric and Conducting Cylinders Using Nanostructured Graphene Metasurfaces. *IEEE Access* **2019**, *7*, 15556–15562. [CrossRef]
72. Arya, A.; Koohestani, M.; Schlinquer, T.; Perdriau, R. A Comprehensive Review of Multiband Electromagnetic Metasurface Structures for Absorption and Wave Manipulation Applications. *IEEE Access* **2026**, *14*, 2973–2997. [CrossRef]
73. Chen, H.T.; Taylor, A.J.; Yu, N. A Review of Metasurfaces: Physics and Applications. *Rep. Prog. Phys.* **2016**, *79*, 076401. [CrossRef]
74. Hamzavi-Zarghani, Z.; Rezaee, B.; Bösch, W.; Matekovits, L. Metasurface-Based Circular Polarization Conversion for a Patch Antenna at 5.8 GHz. In Proceedings of the 2025 International Conference on Electromagnetics in Advanced Applications (ICEAA), Palermo, Italy, 8–12 September 2025; pp. 971–973. [CrossRef]
75. Ghosh, S.; Sainadh, P.M.; Sarkhel, A.; Ghosh, S. Wideband Superstrate-Loaded Metasurface-Based Multifunctional Polarization Converters. *IEEE Antennas Wirel. Propag. Lett.* **2025**, *24*, 1337–1341. [CrossRef]
76. Martinez-de Rioja, D.; Florencio, R.; Martinez-de Rioja, E.; Arrebola, M.; Encinar, J.A.; Boix, R.R. Dual-Band Reflectarray to Generate Two Spaced Beams in Orthogonal Circular Polarization by Variable Rotation Technique. *IEEE Trans. Antennas Propag.* **2020**, *68*, 4617–4626. [CrossRef]
77. Jiang, H.; Song, L.; Guo, L. A Low-Profile and Low-Cost Metal-Only Folded Transmitarray Antenna. *IEEE Antennas Wirel. Propag. Lett.* **2025**, *24*, 1352–1356. [CrossRef]
78. Li, K.; Zhu, C.; Li, L.; Cai, Y.M.; Liang, C.H. Design of Electrically Small Metamaterial Antenna with ELC and EBG Loading. *IEEE Antennas Wirel. Propag. Lett.* **2013**, *12*, 678–681. [CrossRef]
79. Gao, G.P.; Hu, B.; Wang, S.F.; Yang, C. Wearable Circular Ring Slot Antenna with EBG Structure for Wireless Body Area Network. *IEEE Antennas Wirel. Propag. Lett.* **2018**, *17*, 434–437. [CrossRef]
80. Jin, P.; Lin, C.C.; Ziolkowski, R.W. Multifunctional, Electrically Small, Planar Near-Field Resonant Parasitic Antennas. *IEEE Antennas Wirel. Propag. Lett.* **2012**, *11*, 200–204. [CrossRef]
81. Hamzavi-Zarghani, Z.; Grosinger, J. A Near-Field Communication Coil Integrated with a Metasurface. In Proceedings of the 2025 IEEE Wireless Power Technology Conference and Expo (WPTCE), Rome, Italy, 3–6 June 2025; pp. 1–5. [CrossRef]
82. Gomez-Bravo, G.; Guirado, R.; Hödl, P.; Teschl, R.; Perez-Palomino, G.; Witrisal, K.; Wilding, T.; Carrasco, E.; Bösch, W. Utilization of Liquid Crystal Based Reflectarray Antennas for Multipath-Assisted Localization. In Proceedings of the 2024 54th European Microwave Conference (EuMC), Paris, France, 24–26 September 2024; pp. 333–336. [CrossRef]
83. Li, J.; Yang, W.; Ma, S.; Xue, Q.; Che, W. Reconfigurable Millimeter-Wave Tri-Band Antenna Based on VO_2-Films-Embedded Co-Aperture Metasurface Structures. *IEEE Trans. Antennas Propag.* **2023**, *71*, 3134–3145. [CrossRef]
84. Pramanik, S.; Bakshi, S.C.; Koley, C.; Mitra, D.; Monti, A.; Bilotti, F. Active Metasurface-Based Reconfigurable Polarization Converter with Multiple and Simultaneous Functionalities. *IEEE Antennas Wirel. Propag. Lett.* **2023**, *22*, 522–526. [CrossRef]
85. Bilotti, F.; Barbuto, M.; Hamzavi-Zarghani, Z.; Karamirad, M.; Longhi, M.; Monti, A.; Ramaccia, D.; Stefanini, L.; Toscano, A.; Vellucci, S. Reconfigurable intelligent surfaces as the key-enabling technology for smart electromagnetic environments. *Adv. Phys. X* **2024**, *9*, 2299543. [CrossRef]
86. Tian, J.; Yang, H.; Li, T.; Zhang, Z.; Han, J.; Cao, X. Realization and Analysis of Low-Loss Reconfigurable Quasi-Periodic Coding Metasurfaces for Low-Cost Single-Beam Scanning. *IEEE Trans. Microw. Theory Tech.* **2024**, *72*, 5071–5081. [CrossRef]
87. Silaghi, A.M.; Mir, F.; De Sabata, A.; Matekovits, L. Design and Experimental Validation of a Switchable Frequency Selective Surface with Incorporated Control Network. *Sensors* **2023**, *23*, 4561. [CrossRef]
88. White, J.F. PIN Diodes and the Theory of Microwave Operaton. In *Microwave Semiconductor Engineering*; Springer: Dordrecht, The Netherlands, 1982; pp. 39–89. [CrossRef]
89. Cui, C.; Ma, J.; Chen, K.; Wang, X.; Sun, T.; Wang, Q.; Zhang, X.; Zhang, Y. Active and Programmable Metasurfaces with Semiconductor Materials and Devices. *Crystals* **2023**, *13*, 279. [CrossRef]

90. Saikia, M.; Srivastava, K.V. Time Modulation Using Switchable Frequency Selective Surface. In Proceedings of the 2022 IEEE Microwaves, Antennas, and Propagation Conference (MAPCON), Bangalore, India, 12–16 December 2022; pp. 1848–1851. [CrossRef]
91. Li, W.; Guo, H.; Wang, X.; Yang, G.M.; Jin, Y.Q. A 2-bit Reconfigurable Metasurface with Real-Time Control for Deflection, Diffusion, and Polarization. *IEEE Trans. Antennas Propag.* **2024**, *72*, 1521–1531. [CrossRef]
92. Yin, C.; Wang, X.; Yang, G.M.; Jin, Y.Q. Multifunctional Adaptive Invisibility Cloak Based on 3-bit Reconfigurable Metasurface. *IEEE Trans. Antennas Propag.* **2025**, *73*, 8830–8841. [CrossRef]
93. Nesimoglu, T.; Sabah, C. A Tunable Metamaterial Resonator Using Varactor Diodes to Facilitate the Design of Reconfigurable Microwave Circuits. *IEEE Trans. Circuits Syst. II Express Briefs* **2016**, *63*, 89–93. [CrossRef]
94. Yang, X.; Wen, E.; Bharadia, D.; Sievenpiper, D.F. Multifunctional Metasurface: Simultaneous Beam Steering, Polarization Conversion, and Phase Offset. *IEEE Trans. Antennas Propag.* **2024**, *72*, 4589–4593. [CrossRef]
95. Ke, J.C.; Dai, J.Y.; Chen, M.Z.; Wang, L.; Zhang, C.; Tang, W.; Yang, J.; Liu, W.; Li, X.; Lu, Y.; et al. Linear and Nonlinear Polarization Syntheses and Their Programmable Controls Based on Anisotropic Time-Domain Digital Coding Metasurface. *Small Struct.* **2021**, *2*, 2000060. [CrossRef]
96. Costanzo, S.; Venneri, F.; Raffo, A.; Di Massa, G. Dual-Layer Single-Varactor Driven Reflectarray Cell for Broad-Band Beam-Steering and Frequency Tunable Applications. *IEEE Access* **2018**, *6*, 71793–71800. [CrossRef]
97. Rotshild, D.; Rozban, D.; Kedar, G.; Etinger, A.; Abramovich, A. Design and Measurement of a Two-Dimensional Beam-Steerable Metasurface for Ka-Band Communication Systems. *Electronics* **2024**, *13*, 1998. [CrossRef]
98. Tiggelman, M.P.J.; Reimann, K.; Van Rijs, F.; Schmitz, J.; Hueting, R.J.E. On the Trade-Off Between Quality Factor and Tuning Ratio in Tunable High-Frequency Capacitors. *IEEE Trans. Electron Devices* **2009**, *56*, 2128–2136. [CrossRef]
99. Donelli, M.; Iannacci, J.; Manekiya, M. A New Concept of Reconfigurable Antenna Structure Based on an Array of RF-MEMS Switches. *Appl. Sci.* **2024**, *14*, 10941. [CrossRef]
100. Deng, Z.; Wang, Y.; Lai, C. Design and Analysis of Pattern Reconfigurable Antenna Based on RF MEMS Switches. *Electronics* **2023**, *12*, 3109. [CrossRef]
101. Rani, P.; Gaur, M.K.; Tiwari, P.; Kaushik, M.; Shastri, A.; Gahlaut, V. Design and Implementation of a Compact Ultra-Wideband Reconfigurable Antenna Using RF MEMS Switch Technology. *Discov. Electron.* **2025**, *2*, 32. [CrossRef]
102. Shi, Y.; Shen, Z. Recent Advances in Flexible RF MEMS. *Micromachines* **2022**, *13*, 88. [CrossRef]
103. He, S.; Yang, H.; Jiang, Y.; Deng, W.; Zhu, W. Recent Advances in MEMS Metasurfaces and Their Applications on Tunable Lens. *Micromachines* **2019**, *10*, 505. [CrossRef] [PubMed]
104. Si, Y.; Chen, S.; Fu, P.; Yu, J.; Ma, B.; Wu, Q.; Li, M. The Seven-State RF MEMS Miniaturized Broadband Reconfigurable Step Attenuator. *Micromachines* **2024**, *15*, 1182. [CrossRef]
105. Cheng, C.C.; Lakshminarayanan, B.; Abbaspour-Tamijani, A. A Programmable Lens-Array Antenna with Monolithically Integrated MEMS Switches. *IEEE Trans. Microw. Theory Tech.* **2009**, *57*, 1874–1884. [CrossRef]
106. Li, J.; Shah, C.M.; Withayachumnankul, W.; Ung, B.S.Y.; Mitchell, A.; Sriram, S.; Bhaskaran, M.; Chang, S.; Abbott, D. Mechanically tunable terahertz metamaterials. *Appl. Phys. Lett.* **2013**, *102*, 121101. [CrossRef]
107. Zhang, M.; Zhang, W.; Liu, A.Q.; Li, F.C.; Lan, C.F. Tunable Polarization Conversion and Rotation Based on a Reconfigurable Metasurface. *Sci. Rep.* **2017**, *7*, 12068. [CrossRef]
108. Dumas, N.; Trigona, C.; Pons, P.; Latorre, L.; Nouet, P. Design of smart drivers for electrostatic MEMS switches. *Sens. Actuators A Phys.* **2011**, *167*, 422–432. [CrossRef]
109. Chae, U.; Yu, H.Y.; Lee, C.; Cho, I.J. A Hybrid RF MEMS Switch Actuated by the Combination of Bidirectional Thermal Actuations and Electrostatic Holding. *IEEE Trans. Microw. Theory Tech.* **2020**, *68*, 3461–3470. [CrossRef]
110. Alwan, A.; Aluru, N.R. Analysis of Hybrid Electrothermomechanical Microactuators with Integrated Electrothermal and Electrostatic Actuation. *J. Microelectromech. Syst.* **2009**, *18*, 1126–1136. [CrossRef]
111. Petronella, F.; Zaccagnini, F.; Mei, V.D.; Sio, L.D. Liquid crystal metasurfaces. *Liq. Cryst. Rev.* **2025**, *13*, 83–101. [CrossRef]
112. Fritzsch, C.; Wittek, M. Recent developments in liquid crystals for microwave applications. In *Proceedings of the 2017 IEEE International Symposium on Antennas and Propagation & USNC/URSI National Radio Science Meeting, San Diego, CA, USA, 9–15 July 2017*; IEEE: New York, NY, USA, 2017; pp. 1217–1218. [CrossRef]
113. Wang, R.; Zhang, K.; Wei, J.; Zhao, W. Electrically Tunable Generation of Vector Beams via Integrated Liquid Crystal Plates and Dielectric Metasurface. *IEEE Photonics J.* **2025**, *17*, 6801405. [CrossRef]
114. Wang, P.Y.; Sievert, B.; Svejda, J.T.; Benson, N.; Meng, F.Y.; Rennings, A.; Erni, D. A Liquid Crystal Tunable Metamaterial Unit Cell for Dynamic Metasurface Antennas. *IEEE Trans. Antennas Propag.* **2023**, *71*, 1135–1140. [CrossRef]
115. Liu, L.; Deng, L.; Li, S.; Zhang, C.; Wang, L.; Qu, M. Beam Reconfigurable Antenna Based on Liquid Crystal Metasurface. In *Proceedings of the 2018 IEEE 4th International Conference on Computer and Communications (ICCC), Chengdu, China, 7–10 December 2018*; IEEE: New York, NY, USA, 2018; pp. 1037–1041. [CrossRef]

116. Park, J.; Yoo, Y.; Lee, C.; Yoon, D.K.; Park, S.O. Liquid-Crystal-Based Beam-Steering Guided-Wave Metasurface Antenna at Millimeter-Wave Band. *IEEE Antennas Wirel. Propag. Lett.* **2024**, *23*, 4208–4212. [CrossRef]
117. Deng, G.; Zhu, Y.; Zhang, Q.; Yang, J.; Li, Y.; Yin, Z. Reconfigurable Broadband Transmissive-Type Polarization Converter Based on Liquid Crystal Metasurfaces. *IEEE Antennas Wirel. Propag. Lett.* **2025**, *24*, 2327–2331. [CrossRef]
118. Yoo, Y.; Park, J.; Lee, C.; Ki Yoon, D.; Park, S.O. Reconfigurable Multibeam Holographic Antenna Based on Liquid-Crystal Technology for Ka-Band LEO Satellite Application. *IEEE Access* **2025**, *13*, 27141–27149. [CrossRef]
119. Yin, S.; Xiao, D.; Liu, J.; Li, K.; He, H.; Jiang, S.; Luo, D.; Sun, X.W.; Ji, W.; Liu, Y.J. Reconfigurable Chiral Metasurface Absorbers Based on Liquid Crystals. *IEEE Photonics J.* **2018**, *10*, 4600909. [CrossRef]
120. Liu, Y.J.; Si, G.Y.; Leong, E.S.P.; Xiang, N.; Danner, A.J.; Teng, J.H. Light-Driven Plasmonic Color Filters by Overlaying Photoresponsive Liquid Crystals on Gold Annular Aperture Arrays. *Adv. Mater.* **2012**, *24*, OP131–OP135. [CrossRef]
121. Xiao, D.; Liu, Y.J.; Yin, S.; Liu, J.; Ji, W.; Wang, B.; Luo, D.; Li, G.; Sun, X.W. Liquid-crystal-loaded chiral metasurfaces for reconfigurable multiband spin-selective light absorption. *Opt. Express* **2018**, *26*, 25305–25314. [CrossRef] [PubMed]
122. Zhu, M.; Cojocaru-Mirédin, O.; Mio, A.M.; Keutgen, J.; Küpers, M.; Yu, Y.; Cho, J.Y.; Dronskowski, R.; Wuttig, M. Unique Bond Breaking in Crystalline Phase Change Materials and the Quest for Metavalent Bonding. *Adv. Mater.* **2018**, *30*, 1706735. [CrossRef]
123. Wuttig, M.; Deringer, V.L.; Gonze, X.; Bichara, C.; Raty, J.Y. Incipient Metals: Functional Materials with a Unique Bonding Mechanism. *Adv. Mater.* **2018**, *30*, 1803777. [CrossRef]
124. Wang, D.; Zhang, L.; Gong, Y.; Jian, L.; Venkatesan, T.; Qiu, C.W.; Hong, M. Multiband Switchable Terahertz Quarter-Wave Plates via Phase-Change Metasurfaces. *IEEE Photonics J.* **2016**, *8*, 5500308. [CrossRef]
125. Leitis, A.; Heßler, A.; Wahl, S.; Wuttig, M.; Taubner, T.; Tittl, A.; Altug, H. All-Dielectric Programmable Huygens' Metasurfaces. *Adv. Funct. Mater.* **2020**, *30*, 1910259. [CrossRef]
126. Zhang, P.; Fang, B.; Zhao, T.; Li, C.; Shen, C.; Hong, Z.; Jing, X. Terahertz Wave Tunable Metalens Based on Phase Change Material Coded Metasurface. *J. Light. Technol.* **2023**, *41*, 7162–7168. [CrossRef]
127. Wang, J.; Wang, L.; Liu, J. Overview of Phase-Change Materials Based Photonic Devices. *IEEE Access* **2020**, *8*, 121211–121245. [CrossRef]
128. Kats, M.A.; Sharma, D.; Lin, J.; Genevet, P.; Blanchard, R.; Yang, Z.; Qazilbash, M.M.; Basov, D.N.; Ramanathan, S.; Capasso, F. Ultra-thin perfect absorber employing a tunable phase change material. *Appl. Phys. Lett.* **2012**, *101*, 221101. [CrossRef]
129. Wuttig, M.; Bhaskaran, H.; Taubner, T. Phase-change materials for non-volatile photonic applications. *Nat. Photonics* **2017**, *11*, 465–476. [CrossRef]
130. Zhou, Y.; Li, X.; Nie, S.; Sun, P.; Su, L.; Gao, Y. Metamaterial structure design based on genetic algorithm and phase change material GST for multispectral camouflage. *Micro Nanostruct.* **2024**, *195*, 207985. [CrossRef]
131. Ding, F.; Yang, Y.; Bozhevolnyi, S.I. Dynamic Metasurfaces Using Phase-Change Chalcogenides. *Adv. Opt. Mater.* **2019**, *7*, 1801709. [CrossRef]
132. Wu, Y.; Tao, W.; Zhao, F.; Li, C.; Fang, B.; Zhang, P.; Hong, Z.; Jing, X.; Yu, M. Review for metamaterials and metasurfaces based on vanadium dioxide phase change materials. *Opt. Laser Technol.* **2024**, *179*, 111376. [CrossRef]
133. Cotrufo, M.; Sulejman, S.B.; Wesemann, L.; Rahman, M.A.; Bhaskaran, M.; Roberts, A.; Alù, A. Reconfigurable image processing metasurfaces with phase-change materials. *Nat. Commun.* **2024**, *15*, 4483. [CrossRef] [PubMed]
134. Yin, X.; Steinle, T.; Huang, L.; Taubner, T.; Wuttig, M.; Zentgraf, T.; Giessen, H. Beam Switching and Bifocal Zoom Lensing Using Active Plasmonic Metasurfaces. *Light. Sci. Appl.* **2017**, *6*, e17016. [CrossRef]
135. Forouzmand, A.; Mosallaei, H. Dynamic beam control via Mie-resonance based phase-change metasurface: A theoretical investigation. *Opt. Express* **2018**, *26*, 17948–17963. [CrossRef]
136. Zhu, Y.; Vegesna, S.; Zhao, Y.; Kuryatkov, V.; Holtz, M.; Fan, Z.; Saed, M.; Bernussi, A.A. Tunable dual-band terahertz metamaterial bandpass filters. *Opt. Lett.* **2013**, *38*, 2382–2384. [CrossRef]
137. Tittl, A.; Michel, A.K.U.; Schäferling, M.; Yin, X.; Gholipour, B.; Cui, L.; Wuttig, M.; Taubner, T.; Neubrech, F.; Giessen, H. A Switchable Mid-Infrared Plasmonic Perfect Absorber with Multispectral Thermal Imaging Capability. *Adv. Mater.* **2015**, *27*, 4597–4603. [CrossRef]
138. Huitema, L.; Crunteanu, A.; Wong, H.; Arnaud, E. Highly integrated VO_2-based tunable antenna for millimeter-wave applications. *Appl. Phys. Lett.* **2017**, *110*, 203501. [CrossRef]
139. Shafique, K.; Alhassoun, M. Going Beyond a Simple RIS: Trends and Techniques Paving the Path of Future RIS. *IEEE Open J. Antennas Propag.* **2024**, *5*, 256–276. [CrossRef]
140. Popescu, C.C.; Aryana, K.; Mills, B.; Lee, T.W.; Martin-Monier, L.; Ranno, L.; Sia, J.X.B.; Dao, K.P.; Bae, H.B.; Liberman, V.; et al. Unravelling and circumventing failure mechanisms in chalcogenide optical phase change materials. *arXiv* **2024**. [CrossRef]
141. Tripathi, D.; Hegde, R.S. Phase change material metasurface loading enables an ultrafast all-optically switchable, compact, narrowband freespace optical filter. *Opt. Commun.* **2024**, *569*, 130788. [CrossRef]
142. Kumar, K.; Vidal, B.; Garcia-Meca, C. Metasurface based on phase change materials for electrically reconfigurable THz beam steering in copolarized transmission mode. *Sci. Rep.* **2025**, *15*, 40666. [CrossRef]

143. Jeong, J.; Aetukuri, N.; Graf, T.; Schladt, T.D.; Samant, M.G.; Parkin, S.S.P. Suppression of Metal-Insulator Transition in VO_2 by Electric Field—Induced Oxygen Vacancy Formation. *Science* **2013**, *339*, 1402–1405. [CrossRef] [PubMed]
144. Tao, W.; Wu, Y.; Zhao, F.; Li, C.; Fang, B.; Jing, X.; Yu, M. Research progress in metamaterials and metasurfaces based on the phase change material Ge2Sb2Te5. *Opt. Laser Technol.* **2024**, *177*, 111064. [CrossRef]
145. Panda, N.K.; Mohapatra, S.; Sahu, S. Polarization Insensitive Graphene Based Tunable Metasurface Terahertz Dual-Band Absorber. *IEEE Trans. Nanotechnol.* **2025**, *24*, 34–41. [CrossRef]
146. Chen, P.Y.; Alù, A. Terahertz Metamaterial Devices Based on Graphene Nanostructures. *IEEE Trans. Terahertz Sci. Technol.* **2013**, *3*, 748–756. [CrossRef]
147. Hamzavi-Zarghani, Z.; Yahaghi, A.; Matekovits, L.; Peter, I. Tunable Polarization Converter Based on Graphene Metasurfaces. In *Proceedings of the 2018 IEEE Radio and Antenna Days of the Indian Ocean (RADIO), Wolmar, Mauritius, 15–18 October 2018*; IEEE: New York, NY, USA, 2018; pp. 1–2. [CrossRef]
148. Hanson, G.W. Dyadic Green's Functions for an Anisotropic, Non-Local Model of Biased Graphene. *IEEE Trans. Antennas Propag.* **2008**, *56*, 747–757. [CrossRef]
149. Arezoomandan, S.; Gopalan, P.; Tian, K.; Chanana, A.; Nahata, A.; Tiwari, A.; Sensale-Rodriguez, B. Tunable Terahertz Metamaterials Employing Layered 2-D Materials Beyond Graphene. *IEEE J. Sel. Top. Quantum Electron.* **2017**, *23*, 188–194. [CrossRef]
150. Splendiani, A.; Sun, L.; Zhang, Y.; Li, T.; Kim, J.; Chim, C.Y.; Galli, G.; Wang, F. Emerging Photoluminescence in Monolayer MoS_2. *Nano Lett.* **2010**, *10*, 1271–1275. [CrossRef]
151. Tang, B.; Yang, N.; Huang, L.; Su, J.; Jiang, C. Tunable Anisotropic Perfect Enhancement Absorption in Black Phosphorus-Based Metasurfaces. *IEEE Photonics J.* **2020**, *12*, 4500209. [CrossRef]
152. Wan, Y.; Zhang, S.; Jiang, C.; Yun, L.; Wen, J.; Zhang, Z. Optically Tunable Ultrafast Fiber Laser Based on a Ti_3C_2Tx MXene Coated Bandpass Filter. *IEEE Photonics Technol. Lett.* **2025**, *37*, 885–888. [CrossRef]
153. Wang, P.; Han, W.; Peng, L.; Zhang, C.; Wang, Q. Graphene Metasurface Absorber for Traveling Wave Tube Backward Wave Oscillation Suppression. *IEEE Electron Device Lett.* **2025**, *46*, 1624–1627. [CrossRef]
154. Zhang, Y.; Zhao, J.; Zhou, J.; Liu, Z.; Fu, Y. Switchable Polarization Selective Terahertz Wavefront Manipulation in a Graphene Metasurface. *IEEE Photonics J.* **2019**, *11*, 4600909. [CrossRef]
155. Ai, H.; Kang, Q.; Wang, W.; Guo, K.; Guo, Z. Multi-Beam Steering for 6G Communications Based on Graphene Metasurfaces. *Sensors* **2021**, *21*, 4784. [CrossRef] [PubMed]
156. Feng, N.; Zhu, J.; Li, C.; Zhang, Y.; Wang, Z.; Liang, Z.; Liu, Q.H. Near-Unity Anisotropic Infrared Absorption in Monolayer Black Phosphorus with/Without Subwavelength Patterning Design. *IEEE J. Sel. Top. Quantum Electron.* **2019**, *25*, 4700407. [CrossRef]
157. Chen, J.; Wang, J.; Li, X.; Chen, J.; Yu, F.; He, J.; Wang, J.; Zhao, Z.; Li, G.; Chen, X.; et al. Recent Progress in Improving the Performance of Infrared Photodetectors via Optical Field Manipulations. *Sensors* **2022**, *22*, 677. [CrossRef]
158. Esfandiari, M.; Lv, X.; Chamani, S.; Yang, Y. Graphene metasurfaces: Advances in lens applications, design strategies, and fabrication techniques. *Mater. Today Electron.* **2025**, *11*, 100140. [CrossRef]
159. Chou Chau, Y.F. Nanophotonic Materials and Devices: Recent Advances and Emerging Applications. *Micromachines* **2025**, *16*, 933. [CrossRef]
160. Cheng, J.; Fan, F.; Chang, S. Recent Progress on Graphene-Functionalized Metasurfaces for Tunable Phase and Polarization Control. *Nanomaterials* **2019**, *9*, 398. [CrossRef]
161. Han, S.; Kong, J.; Choi, J.; Chegal, W.; Jang, M.S. Single-gate electro-optic beam switching metasurfaces. *Light. Sci. Appl.* **2025**, *14*, 292. [CrossRef]
162. Zeng, C.; Lu, H.; Mao, D.; Du, Y.; Hua, H.; Zhao, W.; Zhao, J. Graphene-empowered dynamic metasurfaces and metadevices. *Opto-Electron. Adv.* **2022**, *5*, 200098. [CrossRef]
163. Thongrattanasiri, S.; Koppens, F.H.L.; García de Abajo, F.J. Complete Optical Absorption in Periodically Patterned Graphene. *Phys. Rev. Lett.* **2012**, *108*, 047401. [CrossRef]
164. Li, A.; Luo, Z.; Wakatsuchi, H.; Kim, S.; Sievenpiper, D.F. Nonlinear, Active, and Tunable Metasurfaces for Advanced Electromagnetics Applications. *IEEE Access* **2017**, *5*, 27439–27452. [CrossRef]
165. ALRikabi, H.T.; Sallomi, A.H.; KHazaal, H.F.; Magdy, A. Design and experimental evaluation of a reconfigurable intelligent surface for wireless applications. *Results Eng.* **2025**, *26*, 104694. [CrossRef]
166. Hao, L.; Vuyyuru, S.K.R.; Tretyakov, S.A.; Salihu, A.; Rupp, M.; Valkonen, R. Modeling RIS From Electromagnetic Principles to Communication Systems—Part II: System-Level Simulation, Ray Tracing, and Measurements. *IEEE Trans. Antennas Propag.* **2025**, *73*, 1756–1767. [CrossRef]
167. Zhu, L.; Mao, H.; Yan, G.; Ma, W.; Xiao, Z.; Zhang, R. Movable and reconfigurable antennas for 6G: Unlocking electromagnetic-domain design and optimization. *npj Wirel. Technol.* **2026**, *2*, 5. [CrossRef]
168. Yu, J.; Jiang, W.; Gong, S. Low-RCS Beam-Steering Antenna Based on Reconfigurable Phase Gradient Metasurface. *IEEE Antennas Wirel. Propag. Lett.* **2019**, *18*, 2016–2020. [CrossRef]

169. Zhang, H.; Chen, X.; Wang, Z.; Ge, Y.; Pu, J. A 1-Bit Electronically Reconfigurable Reflectarray Antenna in X Band. *IEEE Access* **2019**, *7*, 66567–66575. [CrossRef]
170. Li, X.; Sato, H.; Fujikake, H.; Chen, Q. Development of Two-Dimensional Steerable Reflectarray with Liquid Crystal for Reconfigurable Intelligent Surface Applications. *IEEE Trans. Antennas Propag.* **2024**, *72*, 2108–2123. [CrossRef]
171. Ma, Y.; Ma, R.; Lin, Z.; Miao, C.; Zhang, R.; Long, W.; Wu, W.; Wang, J. Distributed Split Single-Sideband Time-Modulated Arrays for Secure Communications. *IEEE Internet Things J.* **2026** . [CrossRef]
172. Hu, X.; Lyu, S.; Zhao, C.; Liu, C.; Peng, M. Distributed IRS Beamforming for Secure Transmission. *IEEE Trans. Veh. Technol.* **2026**, 1–13 . [CrossRef]
173. Trampler, M.E.; Lovato, R.E.; Gong, X. Dual-Resonance Continuously Beam-Scanning X-Band Reflectarray Antenna. *IEEE Trans. Antennas Propag.* **2020**, *68*, 6080–6087. [CrossRef]
174. Nam, Y.H.; Lee, S.G.; Lee, J.H. A Novel Design Method for High-Efficiency Quasi-2-bit Reconfigurable Metasurface Antennas. *IEEE Trans. Antennas Propag.* **2024**, *72*, 4653–4657. [CrossRef]
175. Li, W.; Xia, S.; He, B.; Chen, J.; Shi, H.; Zhang, A.; Li, Z.; Xu, Z. A Reconfigurable Polarization Converter Using Active Metasurface and Its Application in Horn Antenna. *IEEE Trans. Antennas Propag.* **2016**, *64*, 5281–5290. [CrossRef]
176. Zhang, J.; Tao, S.; Yan, X.; Zhang, X.; Guo, J.; Wen, Z. Dual-Frequency Polarized Reconfigurable Terahertz Antenna Based on Graphene Metasurface and TOPAS. *Micromachines* **2021**, *12*, 1088. [CrossRef]
177. Ledimo, B.K.; Moaro, P.; Ramogomana, R.; Mosalaosi, M.; Basutli, B. Design Procedure of a Frequency Reconfigurable Metasurface Antenna at mmWave Band. *Telecom* **2022**, *3*, 379–395. [CrossRef]
178. Cui, T.J.; Liu, S.; Zhang, L. Information metamaterials and metasurfaces. *J. Mater. Chem. C* **2017**, *5*, 3644–3668. [CrossRef]
179. Wan, X.; Qi, M.Q.; Chen, T.Y.; Cui, T.J. Field-Programmable Beam Reconfiguring Based on Digitally Controlled Coding Metasurface. *Sci. Rep.* **2016**, *6*, 20663. [CrossRef] [PubMed]
180. Cao, X.; Deng, C.; Yin, Y.; Hao, Y.; Sarabandi, K. 1-Bit Reconfigurable Transmit- and Reflect-Array Antenna Using Patch-Ground-Patch Structure. *IEEE Antennas Wirel. Propag. Lett.* **2024**, *23*, 434–438. [CrossRef]
181. Wang, M.; Xu, S.; Yang, F.; Li, M. A 1-Bit Bidirectional Reconfigurable Transmit-Reflect-Array Using a Single-Layer Slot Element with PIN Diodes. *IEEE Trans. Antennas Propag.* **2019**, *67*, 6205–6210. [CrossRef]
182. Wan, X.; Xiao, Q.; Zhang, Y.Z.; Li, Y.; Eisenbeis, J.; Wang, J.W.; Huang, Z.A.; Liu, H.X.; Zwick, T.; Cui, T.J. Reconfigurable Sum and Difference Beams Based on a Binary Programmable Metasurface. *IEEE Antennas Wirel. Propag. Lett.* **2021**, *20*, 381–385. [CrossRef]
183. Chen, T.; Song, L.; Liu, Y. A Broadband Dual-Polarized Reconfigurable Transmitarray with Sum and Difference Beam-Steering Capabilities. *IEEE Trans. Antennas Propag.* **2024**, *72*, 8052–8057. [CrossRef]
184. Ramaccia, D.; Monti, A.; Barbuto, M.; Vellucci, S.; Stefanini, L.; Toscano, A.; Bilotti, F. Reconfigurability in Electromagnetic Metasurfaces and Metamaterials for Antenna Systems: State-of-the-art technical approaches, limitations, and applications. [Electromagnetic Metamaterials]. *IEEE Antennas Propag. Mag.* **2025**, *67*, 42–54. [CrossRef]
185. Feng, Y.; Hu, Q.; Qu, K.; Yang, W.; Zheng, Y.; Chen, K. Reconfigurable Intelligent Surfaces: Design, Implementation, and Practical Demonstration. *Electromagn. Sci.* **2023**, *1*, 20111. [CrossRef]
186. Turpin, J.P.; Bossard, J.A.; Morgan, K.L.; Werner, D.H.; Werner, P.L. Reconfigurable and Tunable Metamaterials: A Review of the Theory and Applications. *Int. J. Antennas Propag.* **2014**, *2014*, 429837. [CrossRef]
187. Liu, M.; Wei, R.; Taplin, J.; Zhang, W. Terahertz Metasurfaces Exploiting the Phase Transition of Vanadium Dioxide. *Materials* **2023**, *16*, 7106. [CrossRef]
188. Anagnostou, D.E.; Chryssomallis, M.T.; Braaten, B.D.; Ebel, J.L.; Sepúlveda, N. Reconfigurable UWB Antenna with RF-MEMS for On-Demand WLAN Rejection. *IEEE Trans. Antennas Propag.* **2014**, *62*, 602–608. [CrossRef]
189. Pablo Zapata Cano, H.; Zaharis, Z.D.; Yioultsis, T.V.; Kantartzis, N.V.; Lazaridis, P.I. Pattern Reconfigurable Antennas at Millimeter-Wave Frequencies: A Comprehensive Survey. *IEEE Access* **2022**, *10*, 83029–83042. [CrossRef]
190. Mias, C.; Yap, J.H. A Varactor-Tunable High Impedance Surface with a Resistive-Lumped-Element Biasing Grid. *IEEE Trans. Antennas Propag.* **2007**, *55*, 1955–1962. [CrossRef]
191. Niu, Y.; Li, X.; Zhao, W.; Qi, Z. Polarization-Reconfigurable Low-Profile Antenna Array with 2-Bit Phase Resolution for Beam-Scanning Application. *IEEE Antennas Wirel. Propag. Lett.* **2025**, *24*, 3014–3018. [CrossRef]
192. Wang, R.; Yang, Y.; Makki, B.; Shamim, A. A Wideband Reconfigurable Intelligent Surface for 5G Millimeter-Wave Applications. *IEEE Trans. Antennas Propag.* **2024**, *72*, 2399–2410. [CrossRef]
193. Abdelraouf, O.A.M.; Wang, Z.; Liu, H.; Dong, Z.; Wang, Q.; Ye, M.; Wang, X.R.; Wang, Q.J.; Liu, H. Recent Advances in Tunable Metasurfaces: Materials, Design, and Applications. *ACS Nano* **2022**, *16*, 13339–13369. [CrossRef]
194. Ding, F.; Meng, C.; Bozhevolnyi, S.I. Electrically tunable optical metasurfaces. *Photonics Insights* **2024**, *3*, R07. [CrossRef]
195. Liu, F.; Pitilakis, A.; Mirmoosa, M.S.; Tsilipakos, O.; Wang, X.; Tasolamprou, A.C.; Abadal, S.; Cabellos-Aparicio, A.; Alarcon, E.; Liaskos, C.; et al. Programmable Metasurfaces: State of the Art and Prospects. In *Proceedings of the 2018 IEEE International Symposium on Circuits and Systems (ISCAS)*; IEEE: Piscataway, NJ, USA, 2018; pp. 1–5. [CrossRef]

196. Santonocito, A.; Patrizi, B.; Toci, G. Recent Advances in Tunable Metasurfaces and Their Application in Optics. *Nanomaterials* **2023**, *13*, 1633. [CrossRef] [PubMed]
197. Zhang, Z.; Shi, H.; Wang, L.; Chen, J.; Chen, X.; Yi, J.; Zhang, A.; Liu, H. Recent Advances in Reconfigurable Metasurfaces: Principle and Applications. *Nanomaterials* **2023**, *13*, 534. [CrossRef]
198. Hum, S.V.; Perruisseau-Carrier, J. Reconfigurable Reflectarrays and Array Lenses for Dynamic Antenna Beam Control: A Review. *IEEE Trans. Antennas Propag.* **2014**, *62*, 183–198. [CrossRef]
199. Clemente, A.; Dussopt, L.; Sauleau, R.; Potier, P.; Pouliguen, P. 1-Bit Reconfigurable Unit Cell Based on PIN Diodes for Transmit-Array Applications in *X*-Band. *IEEE Trans. Antennas Propag.* **2012**, *60*, 2260–2269. [CrossRef]
200. Babicheva, V.E.; Kim, H.; Piqué, A. Metasurfaces with Phase-Change Materials for Mid-Wave Infrared Thermal Management. *Micromachines* **2025**, *17*, 17. [CrossRef] [PubMed] [PubMed Central]
201. Wang, L.; Wang, Y.; Zong, G.; Hu, W.; Lu, Y. Liquid crystal based tunable terahertz metadevices. *J. Mater.* **2025**, *11*, 100888. [CrossRef]
202. Singh, T.; Hummel, G.; Vaseem, M.; Shamim, A. Recent Advancements in Reconfigurable mmWave Devices Based on Phase-Change and Metal Insulator Transition Materials. *IEEE J. Microwaves* **2023**, *3*, 827–851. [CrossRef]
203. Hou, Z.; Zhang, Y.; Si, C.; Han, G.; Zhao, Y.; Lu, X.; Liu, J.; Ning, J.; Wei, T. A High-Reliability RF MEMS Metal-Contact Switch Based on Al-Sc Alloy. *Micromachines* **2023**, *14*, 1098. [CrossRef]
204. Wang, Z.; Zhang, N.; Zhang, Y.; Hou, H.; Jin, Y.; Liu, C.; Huang, H.; Guo, Q.; Huang, J.; Cui, Y.; et al. Terahertz MEMS actuators and applications. *Microsyst. Nanoeng.* **2026**, *12*, 69. [CrossRef]
205. Carlson, J.M.; Deshpande, N.V.; Castellanos, M.R.; Heath, R.W. Wideband Dynamic Metasurface Antenna Performance with Practical Design Characteristics. *IEEE Trans. Wirel. Commun.* **2026**, *25*, 4674–4690. [CrossRef]
206. Oliveri, G.; Werner, D.H.; Massa, A. Reconfigurable Electromagnetics Through Metamaterials—A Review. *Proc. IEEE* **2015**, *103*, 1034–1056. [CrossRef]
207. Iqbal, M.; Ashraf, T.; Zubair, M.; Jameel, S.M.; Jazib, M.; Pan, J.Y. A comprehensive survey on reconfigurable intelligent surfaces (RIS) and STAR-RIS for next-generation wireless networks. *Discov. Appl. Sci.* **2025**, *7*, 1253. [CrossRef]
208. Yang, H.Q.; Dai, J.Y.; Li, H.D.; Wu, L.; Shen, Z.H.; Zhou, Q.Y.; Zhang, M.Z.; Wang, S.R.; Wang, Z.X.; Wu, J.W.; et al. Adaptively programmable metasurface for intelligent wireless communications in complex environments. *Nat. Commun.* **2025**, *16*, 6070. [CrossRef] [PubMed]
209. Du, C.; Huang, L. Meta-Reinforcement Learning for Fast Beam Adaptation in 6G Terahertz Reconfigurable Intelligent Surface Communications. *Wirel. Pers. Commun.* **2026**, *146*, 1271–1300. [CrossRef]
210. Zhang, S.; Guo, P.; Jin, H.; Kumar, N.; Zhang, P.; Guizani, M. RIS-Enhanced MEC Framework for Vehicular Networks: Minimizing Delay with Deep Reinforcement Learning. *IEEE Trans. Veh. Technol.* **2025**, 1–12. [CrossRef]
211. Lv, M.; Feng, H.; Jin, Y.; Tian, Y. Advances in Deep Learning-Driven Metasurface Design and Application in Holographic Imaging. *Photonics* **2025**, *12*, 947. [CrossRef]
212. Ma, H.; Park, Q.H. Deep Learning Control of Reconfigurable Metasurface for Real-time Holographic Beam Steering. In Proceedings of the 2023 Conference on Lasers and Electro-Optics (CLEO), San Jose, CA, USA, 7–12 May 2023; pp. 1–2.
213. Yang, Y.; Xin, H.; Liu, Y.; Cheng, H.; Jin, Y.; Li, C.; Lu, J.; Fang, B.; Hong, Z.; Jing, X. Intelligent metasurfaces: Integration of artificial intelligence technology and metasurfaces. *Chin. J. Phys.* **2024**, *89*, 991–1008. [CrossRef]
214. Huang, C.; Zappone, A.; Alexandropoulos, G.C.; Debbah, M.; Yuen, C. Reconfigurable Intelligent Surfaces for Energy Efficiency in Wireless Communication. *IEEE Trans. Wirel. Commun.* **2019**, *18*, 4157–4170. [CrossRef]
215. Liu, Y.; Liu, X.; Mu, X.; Hou, T.; Xu, J.; Di Renzo, M.; Al-Dhahir, N. Reconfigurable Intelligent Surfaces: Principles and Opportunities. *IEEE Commun. Surv. Tutor.* **2021**, *23*, 1546–1577. [CrossRef]
216. Ahmed, M.; Raza, S.; Soofi, A.A.; Khan, F.; Khan, W.U.; Xu, F.; Chatzinotas, S.; Dobre, O.A.; Han, Z. A survey on reconfigurable intelligent surfaces assisted multi-access edge computing networks: State of the art and future challenges. *Comput. Sci. Rev.* **2024**, *54*, 100668. [CrossRef]
217. Tariq, M.; Ahmad, S.; Ahmad Jan, M.; Song, H. Deep Learning Aided Intelligent Reflective Surfaces for 6G: A Survey. *ACM Comput. Surv.* **2024**, *57*. [CrossRef]
218. Sivasankar, S.; Markkandan, S. A Review on Intelligent Reflecting Surfaces: Challenges and Opportunities Towards Secured Communications. *Int. J. Commun. Syst.* **2025**, *38*, e6024. [CrossRef]